AFRL-RI-RS-TR-2008-31
Final Technical Report
February 2008

DATA COMPRESSION TRADE-OFFS FOR TDOA/FDOA GEO-LOCATION SYSTEMS

The Research Foundation of State University of New York, SUNY Binghamton

APPROVED FOR PUBLIC RELEASE; DISTRIBUTION UNLIMITED.

STINFO COPY

AIR FORCE RESEARCH LABORATORY
INFORMATION DIRECTORATE
ROME RESEARCH SITE
ROME, NEW YORK

NOTICE AND SIGNATURE PAGE

AFRL-RI-RS-TR-2008-31 HAS BEEN REVIEWED AND IS APPROVED FOR PUBLICATION IN ACCORDANCE WITH ASSIGNED DISTRIBUTION STATEMENT.

FOR THE DIRECTOR:

/s/	/s/
ANDREW J. NOGA Work Unit Manager	JOSEPH CAMERA, Chief Information & Intelligence Exploitation Division Information Directorate

REPORT DOCUMENTATION PAGE

Form Approved
OMB No. 0704-0188

1. REPORT DATE *(DD-MM-YYYY)*	2. REPORT TYPE	3. DATES COVERED *(From - To)*
FEB 2008	Final	Aug 06 – Jul 07

4. TITLE AND SUBTITLE

DATA COMPRESSION TRADE-OFFS FOR TDOA/FDOA GEO-LOCATION SYSTEMS

5a. CONTRACT NUMBER

5b. GRANT NUMBER
FA8750-06-2-0231

5c. PROGRAM ELEMENT NUMBER
35885G

6. AUTHOR(S)

Mark L. Fowler

5d. PROJECT NUMBER
1038

5e. TASK NUMBER
BA

5f. WORK UNIT NUMBER
02

7. PERFORMING ORGANIZATION NAME(S) AND ADDRESS(ES)
The Research Foundation of State University of New York, SUNY Binghamton
4400 Vestal Parkway E.
Binghamton NY 13902-4514

8. PERFORMING ORGANIZATION REPORT NUMBER

9. SPONSORING/MONITORING AGENCY NAME(S) AND ADDRESS(ES)

AFRL/RIEC
525 Brooks Rd
Rome NY 13441-4505

10. SPONSOR/MONITOR'S ACRONYM(S)

11. SPONSORING/MONITORING AGENCY REPORT NUMBER
AFRL-RI-RS-TR-2008-31

12. DISTRIBUTION AVAILABILITY STATEMENT
APPROVED FOR PUBLIC RELEASE; DISTRIBUTION UNLIMITED. PA# WPAFB 08-0210

13. SUPPLEMENTARY NOTES Resubmission of ADA478488.

14. ABSTRACT
The research results focus on new data compression insights and methods that can enable the sharing of data for enhanced geo-location of RF emitters. The work was focused in four areas: (1) New Theoretical Results: Data compression ideas were applied to the issue of how to select and configure a set of available sensors for location processing. This proved to be a challenging task. (2) Refine & Extend Previous Results: The short-time Fourier transform (STFT) was integrated into the data compression algorithm and was shown to properly operate. (3) Integrate Into a Matlab-based Test-Bed: Matlab routines for data compression were developed and integrated into a single Matlab application. (4) General Location Studies: It was shown that there are issues in using previous results that were developed explicitly for sonar signal cases when the signal was modeled as wide-sense stationary Gaussian process. Results are provided for signal models suitable for the communication signal case.

15. SUBJECT TERMS
Time-Difference of Arrival (TDOA), Frequency-Difference of Arrival (FDOA), Data Compression, Fisher Information

16. SECURITY CLASSIFICATION OF:			17. LIMITATION OF ABSTRACT	18. NUMBER OF PAGES	19a. NAME OF RESPONSIBLE PERSON
a. REPORT	b. ABSTRACT	c. THIS PAGE			Andrew J. Noga
U	U	U	UL	42	19b. TELEPHONE NUMBER (*Include area code*) N/A

Abstract: The research results reported on here focus on new data compression methods that can enable Air Force systems to more rapidly and effectively share data for precision geolocation of RF emitters. The work was focused in four areas:
(1) New Theoretical Results: We extend the previous rudimentary insight into how to use data compression to accomplish trade-offs between the sequence of tasks in a location processing scenario. In addition, data compression ideas were applied to the issue of how to select and configure a set of available sensors for location processing. This proved to be a challenging task.
(2) Refine & Extend Previous Results: The short-time Fourier transform (STFT) was integrated into the data compression algorithm and was shown to properly operate.
(3) Integrate Into a Matlab-based Test-Bed: Matlab routines for data compression were developed and integrated into a single Matlab application.
(4) General Location Studies: In support of AFRL emitter location system development activities, this report provides important insight into the suitability of the use of previous results on emitter location. In particular, it was shown that there is a danger in using previous results that were developed explicitly for the sonar signal case when the signal was modeled as a wide-sense stationary Gaussian process. Results are provided for signal models suitable for the communication signal case.

Keywords: Emitter Location, Time-Difference-of-Arrival, Frequency-Difference-of-Arrival, Data Compression, Fisher Information, Sensor Selection, Signal Model

Table of Contents

List of Figures

List of Symbols, Abbreviations and Acronyms

AFRL	Air Force Research Laboratory
CRLB	Cramer-Rao Lower Bound
FDOA	Frequency-Difference-of-Arrival
FIM	Fisher Information Matrix
ML	Maximum Likelihood
PDF	Probability Density Function
SNR	Signal-to-Noise Ratio
STFT	Short Time Fourier Transform
TDOA	Time-Difference-of-Arrival
UAV	Unmanned Aerial Vehicle
C_k^n	The number of ways k items can be chosen from n items
R	Allocated number of bits for compression; subscripts identify allocations for different tasks
σ^2	Variance of noise; subscripts indicate different noise sources
τ	TDOA variable
ω	FDOA variable
$\hat{\tau}$	TDOA estimate
$\hat{\omega}$	FDOA estimate
$\Delta\tau$	Error in TDOA estimate
$\Delta\omega$	Error in FDOA estimate
$\mathbf{G}_i$	Geometry matrix; subscript indicates sensor pair
$\mathbf{J}_{geo}$	Fisher information matrix for the geolocation estimate
$\mathbf{FI}_m$	Fisher information matrix for the TDOA/FDOA estimate of the m^{th} pair
$\mathbf{F}_\theta$	Fisher information matrix for the all the TDOA/FDOA estimates
$\mathbf{X} \sim N(\boldsymbol{\mu},\mathbf{C})$	Notation indicating that random vector $\mathbf{X}$ is normally distributed (i.e., Gaussian) with mean vector $\boldsymbol{\mu}$ and covariance matrix $\mathbf{C}$

1 Introduction

Since a primary task of multi-sensor systems (including emitter location systems) is to make statistical inferences based on the data collected throughout the sensor system, it is important to design compression methods that cause minimal degradation of the quality of these inferences. Although data compression for distributed sensor systems *has* been previously considered by others to some degree, an important aspect not considered in other researcher's work is that sensor systems may have multiple inference tasks to accomplish (either simultaneously or sequentially). Multiple inferences generally have conflicting compression requirements and finding the right way to balance these conflicts is crucial. For example, we have demonstrated that in a TDOA/FDOA[1]-based location system there is a conflict between compressing for TDOA accuracy vs. FDOA accuracy. Thus, trade-offs between TDOA/FDOA accuracy must be made. However, because this trade-off depends on the relative geometry between emitter and receivers, it is not known a priori where the proper operating point within this trade-off should be; we have developed a way to address that geometry-dependent trade-off [1].

There are also trade-offs between multiple sequential inferences. As an example of multiple inferences, consider the case where multiple sensors are deployed to detect and then locate RF emitters. This is a case of multiple sequential inferences where the compression can be done sequentially as well. Overall then, a need exists for compression that is optimized to handle sequential and/or simultaneous inference tasks. We had previously developed some preliminary results addressing this need [1]; here those results are extended.

We have demonstrated that one of the keys to addressing the sequential and simultaneous task viewpoint is to use distortion measures that accurately reflect the ultimate performance on the tasks. For estimation tasks the ultimate performance is the variance of the estimation error (at least in the unbiased estimate case). For decision tasks the ultimate performance is the probability of detection for a given false-alarm probability. To design compression algorithms with respect to these performance goals it is essential to have appropriate, useable metrics that measure the impact of reducing the rate on the inference performance. Our approach uses specific distortion measures to assess the impact of compression on the multiple inferences: Fisher information is used to assess the impact on estimation accuracy while Chernoff and Kullback-Liebler distances are used to assess the impact on decision accuracy. Although these inference-centric distortion measures have been applied before, it has been for single-inference cases; the real interest here is to explore how these measures are used to address the data compression *trade-offs* for *multiple* sequential and simultaneous inferences – namely, the case of "detect-then-locate" for RF communication emitters.

We have also addressed the data compression trade-offs in *simultaneous* estimation of TDOA and FDOA using compressed data from one sensor and local data from a second sensor [1]. We have derived the Fisher information-based distortion measure for these two estimates and found that the TDOA measure is best optimized in the frequency domain while the FDOA measure is best optimized in the time domain. To address data compression trade-offs for the *simultaneous* estimation of TDOA/FDOA requires the use

[1] TDOA = Time-Difference-of-Arrival and FDOA = Frequency-Difference-of-Arrival

of a time-frequency representation and we have used a wavelet packet approach. Furthermore, this case requires using the Fisher information matrix (FIM); we have found that the approach of maximizing the trace of the FIM yields good results. We showed that it is not possible to know *a priori* the proper trade-off point between TDOA and FDOA because it depends on the (unknown) geometry between emitter and sensors; however, we have proposed a "geometry adaptive" scheme that sets the compression algorithm's trade-off point based on a small amount of initial data sent compressed for the equal trade-off case.

In [1] these ideas have been refined and extended to include more geometric aspects as well as to include preliminary results on the data compression trade-offs for the *sequential* "detect-then-locate" problem – although these sequential results were limited to the TDOA-only location case rather than the more general joint TDOA/FDOA-based location case. In addition, we have addressed issues surrounding the use of the short-time Fourier transform (STFT) for evaluating the Fisher information contributions of the collected data for the purpose of TDOA/FDOA estimation.

The results presented in this report extend the results described above as follows. The work was focused in four areas:

(1) New Theoretical Results: We extend the previous rudimentary insight into how to use data compression to accomplish trade-offs between the sequence of tasks in a location processing scenario. In addition, data compression ideas were applied to the issue of how to select and configure a set of available sensors for location processing. This proved to be a challenging task.

(2) Refine & Extend Previous Results: The short-time Fourier transform (STFT) was integrated into the data compression algorithm and was shown to properly operate.

(3) Integrate into a Matlab-based Test-Bed: Matlab routines for data compression were developed and integrated into a single Matlab application.

(4) General Location Studies: In support of AFRL emitter location system development activities, this report provides important insight into the suitability of the use of previous results on emitter location. In particular, it was shown that there is a danger in using previous results that were developed explicitly for the sonar signal case when the signal was modeled as a wide-sense stationary Gaussian process. Results are provided for signal models suitable for the communication signal case.

2 New Theoretical Results

2.1 Sequential Detect-Then-Location

The scenario to be considered here is:

- Receive signals at two receivers: Collect a fixed, specified number of samples (a "block of samples")
- Compress and share parts of the data to support detection of a common signal at the two receivers
- Once detected… compress and share parts of the data to support estimation of the TDOA/FDOA.

This method uses the generalized likelihood ratio test derived for this problem in Prof. Fowler's Final Report for his Summer 2005 Summer Faculty Fellowship at AFRL. The generalized likelihood ratio test is then used to determine the proper distortion measure relative to which the compression algorithm will be optimized for the detection task. As shown in the Summer 2005 final report, the part of the measure that captures impact of compression on the detection performance is the post-compression/pre-detection SNR. Then we will briefly show how to use this to address compression for sequential detect-then-TDOA/FDOA processing.

Thus, the framework we now work under is that we will use SNR as the compression distortion measure for the detection task and we will use the TDOA/FDOA Fisher information given in [1].

2.1.1 An Algorithm for Sequential Detect-Then-TDOA/FDOA

Stage 1: Maximizing SNR for the Detection Task

The signal (having N samples) to be compressed is decomposed using a wavelet packet transform whose N coefficients are given by $\{c_n\}_{n=0}^{N-1}$. The allocation of bits to these coefficients is done on a block basis, where each block consists of temporally adjacent wavelet cells at the same frequency; the number of cells in a block is typically chosen to be 8. Let $\{b_1(n)\}_{n=0}^{N-1}$ be the Stage 1 allocation of bits to the coefficients; note that due to the block basis allocation $b_1(n)$ is constant over all values of n within a given block. Let $q^2(b_1(n))$ be the quantization noise variance of the n^{th} coefficient when allocated $b_1(n)$ bits. Let f_n^2 be the frequency of the n^{th} coefficient and let t_n^2 be the time centroid *of the block* containing the n^{th} coefficient. Let σ^2 be the variance of the noise in the received signal before compression. Then the Stage 1 compression seeks to

$$\underset{\{b_1(n)\}_{n=0}^{N-1}}{\textit{Maximize}} \left[(1-\beta)\sum_{n=0}^{N-1} \frac{|c_n|^2}{\sigma^2 + q^2(b_1(n))} + \beta\left(\alpha\sum_{n=0}^{N-1}\left(\frac{f_n^2 |c_n|^2}{\sigma^2 + q^2(b_1(n))} \right) + (1-\alpha)\sum_{n=0}^{N-1}\left(\frac{t_n^2 |c_n|^2}{\sigma^2 + q^2(b_1(n))} \right) \right) \right] \quad (1)$$

$$\text{subject to} \quad \sum_{n=0}^{N-1} b_1(n) \le R_D$$

where R_D is bit budget for Stage 1, and the parameter β controls the tradeoff between detection and TDOA/FDOA estimation while the parameter α controls the tradeoff between TDOA and FDOA accuracy (see [1]). The second two summation terms in (1) measure the importance of a bit for TDOA/FDOA estimation while the first summation measures the importance of the bit for detection. Thus, setting $\beta = 0$ causes this allocation to be done with no consideration of the Stage 2 task of TDOA/FDOA estimation; however, increasing β forces more consideration of the subsequent Stage 2 task.

Stage 2: Maximizing Fisher Information for the TDOA/FDOA Estimation Task

In this stage the detection processing has been completed and only TDOA/FDOA is of interest and its accuracy needs to be refined by sending additional bits allocated to the wavelet packet coefficients. Let $\{b_2(n)\}_{n=0}^{N-1}$ be the additional bits allocated during Stage 2 so that the quantization noise variance of the n^{th} coefficient now becomes $q^2(b_1(n)+b_2(n))$. Thus, the Stage 2 compression optimization seeks to

$$\underset{\{b_2(n)\}_{n=0}^{N-1}}{\text{Maximize}} \left[\left(\alpha \sum_{n=0}^{N-1} \left(\frac{f_n^2 |c_n|^2}{\sigma^2 + q^2(b_1(n)+b_2(n))} \right) + (1-\alpha) \sum_{n=0}^{N-1} \left(\frac{t_n^2 |c_n|^2}{\sigma^2 + q_j^2(b_1(n)+b_2(n))} \right) \right) \right] \quad \text{subject to} \quad \sum_{n=0}^{N-1} b_2(n) \le R_E \tag{2}$$

where R_E is bit budget for Stage 2.

Comparing this to the results in the Summer 2005 Final Report shows that (1) and (2) are simple modifications of the detect-then-TDOA algorithm and are expected to behave similarly. No further effort was made to pursue this avenue because of its similarity to the earlier ideas; instead this effort was re-directed to the sensor selection problem because it turned out to be more challenging than expected.

2.2 Sensor Selection and Configuration

Multiple sensors can locate an emitter by sharing data between pairs of sensors and computing time/frequency-difference-of-arrival (TDOA/FDOA). We address optimal selection of a subset of sensors to reduce the needed network capacity. Fisher information can be used to assess the data quality across multiple sensors to manage the network of sensors to optimize the location accuracy subject to communication constraints. From an unconstrained-resources viewpoint it is desirable to use the complete set of deployed sensors; however, that generally results in an excessive data volume. Selecting a subset of sensors to participate in a sensing task is crucial to satisfying trade-offs between accuracy and time-line requirements. For emitter location it is well-known that the geometry between sensors and the target plays a key role in determining the location accuracy. Furthermore, the deployed sensors have different data quality. Given these two factors, it is no trivial matter to select the optimal subset of sensors.

We propose various approaches to this problem and discuss trade-offs between them. The first method assumes that the sensors have pre-paired and share their data between these pairs; sensor selection then consists of selecting pairs to optimize performance while meeting constraints on number of pairs selected. The second method consists of optimally determining pairings as well as selections of pairs but with the constraint that no sensors are shared between pairs. The third method consists of allowing sensors to be shared between pairs.

We discuss several aspects of these three methods. The first method is simple to solve but clearly the pre-pairing requirement makes this method clumsy and very sub-optimal. In the second method, it is simple to evaluate the Fisher information but is challenging to make the optimal selections of sensors. However, in the third method

things are reversed in that it is more challenging to evaluate the Fisher information but is simple to make the optimal selections of sensors.

Our general interest is in achieving network-wide optimization over a large number of simultaneously deployed sensors to enable more efficient and effective cooperation within the network of sensors.

We consider the specific scenario of using the sensors to locate a non-cooperative RF emitter by TDOA/FDOA-based methods; here TDOA refers to Time-Difference-of-Arrival and FDOA to Frequency-Difference-of-Arrival, which can be jointly estimated by cross-correlating signals from a pair of the sensors. The accuracy of the TDOA/FDOA estimates depends on the signal SNR and the time-frequency structure of the intercepted signal; however, the accuracy of the location estimation depends also on the emitter/sensor geometry. The goal of our work is to optimize over the set of all sensor assets, under the constraint of limited network communication resources.

2.2.1 Problem Description

For simplicity we consider only the 2-D geometrical scenario. In the scenario we consider a rough estimate of emitter location has already been made (either by our system or by a cueing system). As shown in Figure 1, we wish to find the location of a stationary emitter, denoted by $\mathbf{u} \equiv [x_e, y_e]^T$, using signals intercepted at N unmanned aerial vehicle (UAV) sensors denoted S1 to SN, whose positions are $\mathbf{x}_i \equiv [x_i, y_i]^T$ and speeds are $\dot{\mathbf{x}}_i \equiv [\dot{x}_i, \dot{y}_i]^T$, for $i = 1,2,\ldots,N$.

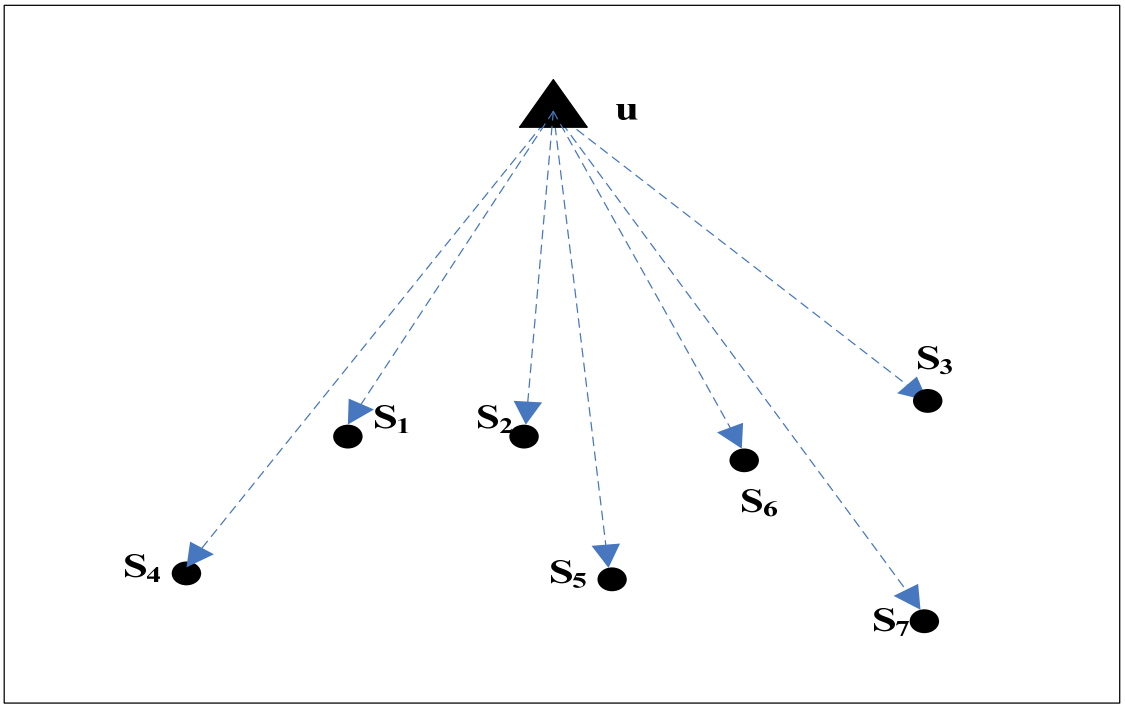

Figure 1 Geometry for stationary source location

Let r_i denote the Euclidean distance between the emitter and the i^{th} sensor S_i; that is

$$r_i = |\mathbf{x}_i - \mathbf{u}| = \sqrt{(x_i - x_e)^2 + (y_i - y_e)^2} \ . \tag{3}$$

To compute the TDOA/FDOA measurements the sensors must be paired. We consider three types of pairings within the network of sensors, as shown in Figure 2.

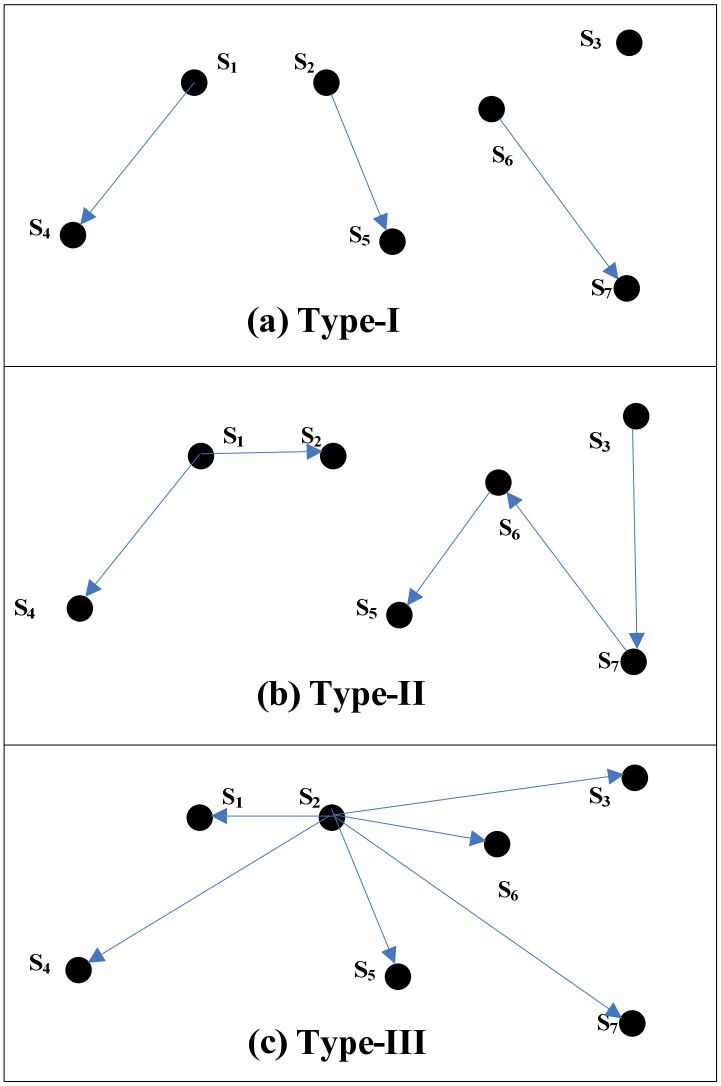

Figure 2 Three types of sensor network

(1) Type-I: No Sensor Sharing (two pairs that do not share a sensor are said to be "independent pairs");

(2) Type-II: De-Centralized Sensor Sharing (i.e., sensors are shared between pairs but no sensor is part of more than two pairs);

(3) Type-III: Centralized Sensor Sharing (i.e., a common reference sensor is used).

For the i^{th} pair of sensors the TDOA τ_i and FDOA ω_i between the signals received at the two sensors in the pair are given by

$$\begin{aligned}\tau_i &= \frac{1}{c}\left(r_{i,1} - r_{i,2}\right) \\ \omega_i &= \frac{f_e}{c}\left(\mathbf{u}_{i,1}^T \cdot \dot{\mathbf{x}}_{i,1} - \mathbf{u}_{i,2}^T \cdot \dot{\mathbf{x}}_{i,2}\right),\end{aligned} \tag{4}$$

where $\mathbf{u}_{i.k}$ is the unit vector pointing from the k^{th} sensor in the i^{th} pair to the emitter, for $k = 1,2$, and f_e is the transmitted frequency of the transmitter (assumed estimated in advance).

Assume there are M pairs totally. Let $\boldsymbol{\theta}_m = [\tau_{k_m j_m}, \omega_{k_m j_m}]^T$ be the parameter vector to be estimated by the m^{th} pair of sensors, which is paired by $(k_m)^{th}$ and $(j_m)^{th}$ sensors, where $m = 1,2,\ldots,M$; and $k_m j_m \in \{1,2,...,N\}, k_m \neq j_m$. Let $\hat{\tau}_{k_m j_m}$ and $\hat{\omega}_{k_m j_m}$ be the estimates, $\Delta\tau_{k_m j_m}$ and $\Delta\omega_{k_m j_m}$ be the estimation errors, then

$$\begin{aligned}\hat{\tau}_{k_m j_m} &= \tau_{k_m j_m} + \Delta\tau_{k_m j_m} \\ \hat{\omega}_{k_m j_m} &= \omega_{k_m j_m} + \Delta\omega_{k_m j_m}\end{aligned} \tag{5}$$

Because the estimate $\hat{\boldsymbol{\theta}}_m$ is obtained by maximum likelihood (ML) estimator [16], the asymptotic properties of ML estimators [17] gives that the PDF of it is Gaussian with covariance matrix that is the inverse of the Fisher information matrix (FIM), so

$$\begin{bmatrix}\Delta\tau_{k_m j_m} \\ \Delta\omega_{k_m j_m}\end{bmatrix} \sim N(0, \mathbf{FI}_m^{-1}) \tag{6}$$

As we know $\mathbf{FI}_m$ depends only on the sensors received signals according to [17]

$$\mathbf{FI}_m = 2\,\mathrm{Re}\left[\frac{\partial \mathbf{s}_m^H(\boldsymbol{\theta}_m)}{\partial \boldsymbol{\theta}_m}\boldsymbol{\Sigma}_m^{-1}\frac{\partial \mathbf{s}_m(\boldsymbol{\theta}_m)}{\partial \boldsymbol{\theta}_m}\right], \tag{7}$$

where $\mathbf{s}_m$ is the vector of received signals and $\boldsymbol{\Sigma}_m$ is the covariance of the AWGN at the m^{th} sensor pair. The FIM of $\boldsymbol{\theta} = [\boldsymbol{\theta}_1^T, \boldsymbol{\theta}_2^T, \ldots, \boldsymbol{\theta}_M^T]^T$ has a block structure as

$$\mathbf{F}_\theta = \begin{bmatrix}\mathbf{FI}_1 & \mathbf{I}_{12} & \cdots & \mathbf{I}_{1M} \\ \mathbf{I}_{21} & \mathbf{FI}_2 & \ddots & \mathbf{I}_{2M} \\ \vdots & \ddots & \ddots & \vdots \\ \mathbf{I}_{M1} & \mathbf{I}_{M2} & \cdots & \mathbf{FI}_M\end{bmatrix}, \tag{8}$$

where $\mathbf{I}_{m,k}$ is the cross term FIM between m^{th} and k^{th} pairs, which is evaluated in Section 2.2.5.

The TDOA/FDOA estimates are then used by the sensor system to estimate the location of the emitter. Because of the asymptotic properties of the ML estimator of TDOA/FDOA we can take the TDOA/FDOA estimates as Gaussian so that the FIM of the estimate of the geo-location is given by [18]

$$\mathbf{J}_{geo} = \left[\mathbf{G}_1^{\mathrm{T}}, \cdots, \mathbf{G}_m, \cdots, \mathbf{G}_M^{\mathrm{T}}\right] \mathbf{F}_\theta \begin{bmatrix} \mathbf{G}_1 \\ \vdots \\ \mathbf{G}_M \end{bmatrix}, \tag{9}$$

where $\mathbf{G}_m$ is the Jacobian matrix of the m^{th} pair of sensors, defined by $\mathbf{G}_m = \dfrac{\partial \boldsymbol{\theta}_m(\mathbf{u})}{\partial \mathbf{u}}$ and calculated by

$$\mathbf{G}_m = \begin{bmatrix} (\mathbf{x}_{k_m} - \mathbf{u})^T / r_{k_m} - (\mathbf{x}_{j_m} - \mathbf{u})^T / r_{j_m} \\ (\mathbf{x}_{k_m} - \mathbf{u})^T \dot{\mathbf{r}}_{k_m} / r_{k_m}^2 - (\mathbf{x}_{j_m} - \mathbf{u})^T \dot{\mathbf{r}}_{j_m} / r_{j_m}^2 - \dot{\mathbf{x}}_{k_m}^T / r_{k_m} + \dot{\mathbf{x}}_{j_m}^T / r_{j_m} \end{bmatrix}. \tag{10}$$

Our objective is to select an optimal subset of sensors and pair them as well. The criterion we used to make the decision is the trace of FIM of geo-location [18],[19] as

$$\max_{\text{all possible subset solutions}} \left\{ trace(\mathbf{J}_{geo}(\text{subset})) \right\} \tag{11}$$

In the following sections, we discuss sensor selection algorithms for the three network types.

2.2.2 Algorithms

2.2.2.1 Pre-Paired Sensors

When sensors are pre-paired, we simply select pairs instead of sensors. The FIM $\mathbf{FI}_m$ and cross-FIM $\mathbf{I}_{m,k}$ are evaluated based on the paring and sensor sharing.

Type-I: No Sensor Sharing—When no sensor is shared the cross-FIMs $\mathbf{I}_{m,k}$ are zero. The $\mathbf{FI}_m$ are evaluated individually for each pair. Then $\mathbf{F}_\theta$ will have block diagonal structure as

$$\mathbf{F}_\theta = \begin{bmatrix} \mathbf{FI}_1 & \mathbf{0} & \cdots & \mathbf{0} \\ \mathbf{0} & \mathbf{FI}_2 & \ddots & \mathbf{0} \\ \vdots & \ddots & \ddots & \vdots \\ \mathbf{0} & \mathbf{0} & \cdots & \mathbf{FI}_M \end{bmatrix} \tag{12}$$

The problem of selecting K sensor pairs from N pairs is specified by

$$\max_{p_1,\cdots,p_N} \{trace(p_1(\mathbf{G}_1^T\mathbf{F}\mathbf{I}_1\mathbf{G}_1)+\cdots+p_N(\mathbf{G}_N^T\mathbf{F}\mathbf{I}_N\mathbf{G}_N))\}$$
$$s.t.\quad p_1+\cdots+p_N=K<N,\quad p_i\in\{0,1\} \tag{13}$$

The solution of this was discussed in [19]: we simply select the K pre-paired sensor pairs that have the largest values of

$$trace\{\mathbf{J}_{geo,k}\}=trace\{\mathbf{G}_k^T\mathbf{F}\mathbf{I}_k\mathbf{G}_k\}\,. \tag{14}$$

Type-II: De-Centralized Sensor Sharing—Here we treat sensors by sensor sets, where a sensor set is defined as a group of sensors which have no connections to sensors outside the group and do not have any independent pairs inside the group. For the sensor network in Figure 2 (b), the sets are defined as in Figure 3.

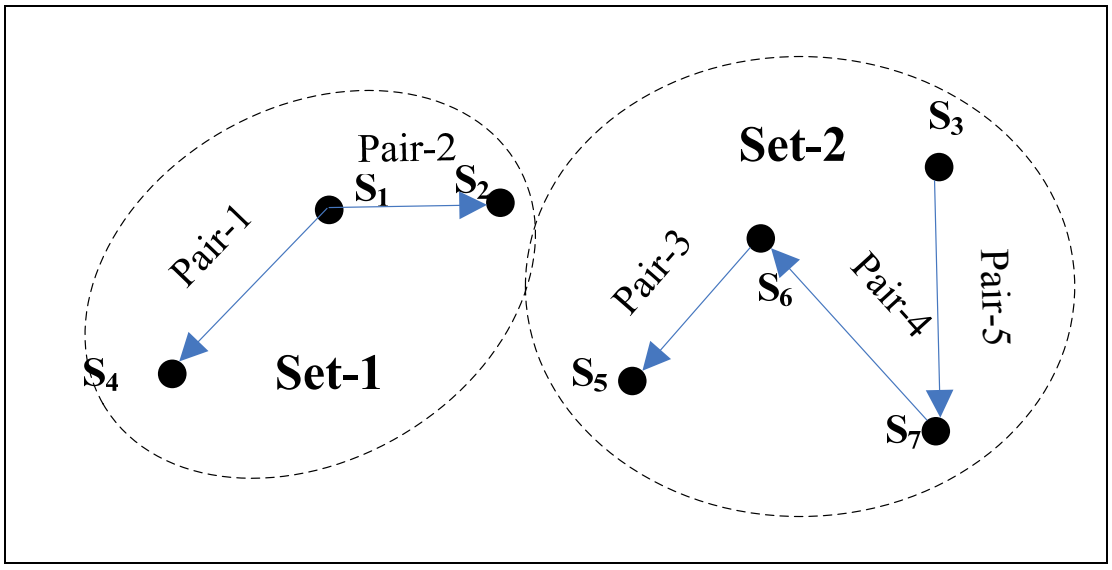

Figure 3 Sensor sets example

The geo-location FIM of each sensor set is computed; for example, the evaluation of set-1 is

$$\mathbf{J}_{geo,set-1}=\mathbf{G}_1^T\mathbf{F}\mathbf{I}_1\mathbf{G}_1+\mathbf{G}_2^T\mathbf{F}\mathbf{I}_2\mathbf{G}_2+2\mathbf{G}_1^T\mathbf{I}_{1,2}\mathbf{G}_2\,. \tag{15}$$

Then the problem of selecting K sensors from M sets is specified by

$$\max_{p_1,\cdots,p_N} \{trace(p_1\cdot\mathbf{J}_{geo,set-1}+\cdots+p_M\cdot\mathbf{J}_{geo,set-M})\}$$
$$s.t.\quad p_1\cdot n_1+\cdots+p_1\cdot n_M=K<N,\quad p_i\in\{0,1\} \tag{16}$$
$$n_i \text{ is the number of sensors in set-i}$$

and can be easily solved. For example, if we are asked to select 5 sensors, we can check the set which has 5 sensors, or the two sets which have 2 sensors and 3 sensors respectively, and add the trace of the two sets up, compare it with the one with 5 sensors and choose the larger one.

Type-III: Centralized Sensor Sharing—For the pre-paired case, the central sensor is already specified and the remaining $N-1$ sensors pair with it to form $N-1$ centralized pairs. There are C_{N-1}^{K} possible ways to select K pairs. The FIM of this set will have the following structure

$$\mathbf{J}_{geo,k} = \sum_{k=1}^{K} \mathbf{G}_k^{\mathrm{T}} \mathbf{F}\mathbf{I}_k \mathbf{G}_k + \sum_{m=1,k=m+1}^{m=K-1,k=K} 2\mathbf{G}_m^{\mathrm{T}} \mathbf{I}_{m,k} \mathbf{G}_k \,. \tag{17}$$

If the r^{th} sensor is the reference sensor then Section 2.2.5 states that $\mathbf{F}\mathbf{I}_k = \mathbf{F}_k + \mathbf{F}_r$ and $\mathbf{I}_{m,k} \equiv \mathbf{F}_r$. In this case, we have to evaluate the trace of all the FIMs of geo-location of the C_{N-1}^{K} possible combinations, and choose the largest one:

$$\begin{aligned} &\max_{set,k \in \{C_{N-1}^{K}\}} \{trace(\mathbf{J}_{set,k})\} \\ &\{C_{N-1}^{K}\} \text{ is all the possible combination set} \end{aligned} \tag{18}$$

2.2.2.2 Non-Pre-Paired Sensors

We are given a set of sensors and asked to optimally choose a subset and the optimal pairings as well. In this case the pairing provides more flexibility to enable better performance but it introduces additional complexity as well.

Type-I Pairing of Sensors: No Sensor Sharing—For N sensors, there could be $N/2$ independent pairs. To choose $K(\le N/2)$ pairs is a time-consuming work if we enumerated all the possible solutions. For example, $N=10$, there are $C_{10}^{2}=45$ possible pairs, and $(N-1)\cdot(N-3)\cdots 3\cdot 1 = 945$ possible ways to make 5 pairs as a subset. Fortunately, since there is no sensor sharing and we select sensors pair by pair, the selection of the next pair will not affect the selection of the previous one. This yields a tree structure and allows use of integer dynamic programming method [2]. For this paper we used the "Branch and Bound" method to choose a pair at each step. The objective function is

$$\max_{all\ feasible\ solutions} \left\{ \sum_{k=1}^{K} trace(\mathbf{J}_{geo,k^{th}\ pair\ in\ the\ solution}) \right\} \tag{19}$$

A "feasible solution" means any selection/pairing of sensors where no sensors are shared and the selected number of sensors is as required. Section 2.2.6 illustrates a simple example of this method.

Type-II Pairing of Sensors: De-Centralized Sensor Sharing—For N sensors, there could be C_N^2 possible pairs. To choose $K(\le C_N^2)$ pairs, there are $C_{C_N^2}^K$ possible ways to pair and then select K pairs. For example, for $N=10, K=5$, the number of ways is 122,1759, which is quite large and nonconductive to listing all of them. But fortunately, among all this large number of ways to pair and select, only a small number of them are unique. We have established the following theorem which is proved in Section 2.2.7.

Theorem*: For N sensors, at most independent N-1 pairs can be used as a "sensor set"; and different pairing methods of the N sensors to make N-1 independent pairs will result in the same CRLB of geo-location.*

We can exploit this result to simplify the optimal selection and pairing for this case. When we are given N sensors and asked to make K pairs, there are many solutions for this network. We can use at least $K+1$ sensors to make it or at most $2K$. Since the main advantage to share sensors is to save some sensor energies, we would like to use the number of sensors as less as possible. So here we only choose $K+1$ sensors to make K pairs.

For example, for given $N=7$ and $K=3$ pairs needed, compute the FIM of geo-location of all $C_7^4=35$ solutions, and find the one with the largest trace. Inside each solution, sensors are "paired by sequence." For example, as in Figure 4, the solution set is $\{S_4, S_1, S_2, S_5\}$.

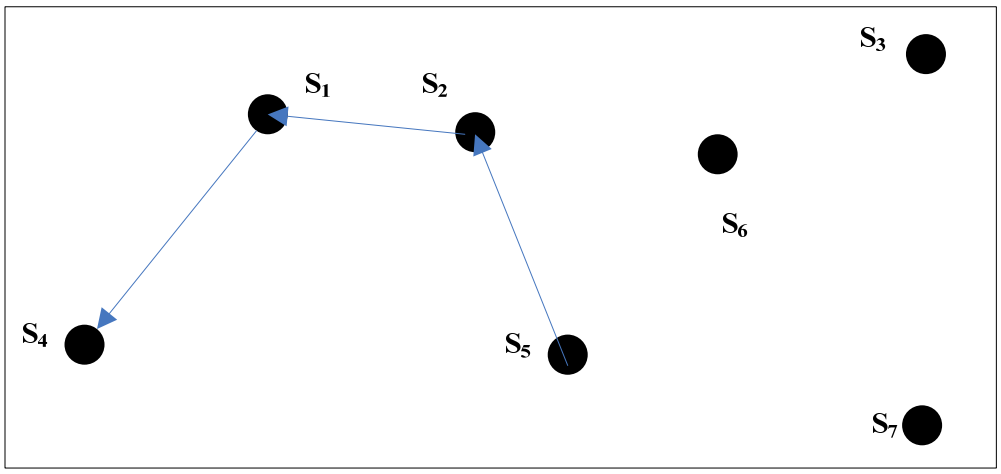

Figure 4 An example of pairing by sequence

2.2.3 Simulation Results

To demonstrate the capability of the sensor selection methods we present some simulation results for the case of locating an emitter with a random lay-down of 14 sensors. The sensor selection proceeds as follows. Each sensor intercepts the emitter signal data at SNRs in the range of 10~15dB (where the SNR variation is assumed to depend quadratically on the range to the emitter). The full set of sensors share a very small amount of data to obtain a rough estimate of the emitter location; alternatively, we

could consider the case where the system is cued by some other sensor system that provides a rough location that is to be improved using our sensors.

Figure 5 shows the performance of sensor selections without sensor sharing. We select 6 to 14 sensors to make 3 to 7 pairs, shown on the horizontal axis. The vertical axis shows the standard deviation of the geo-location error versus the number of sensors/pairs selected. The upper curve (-Δ-) shows the performance for the pre-paired sensor case without sharing; the lower curve (-O-) shows the performance when using the selection and pairing method discussed above for the case of no sensor sharing. Not surprisingly, the ability to select the pairing on the basis of the sensor geometry and the rough emitter location enables better performance than using pre-paired sensors.

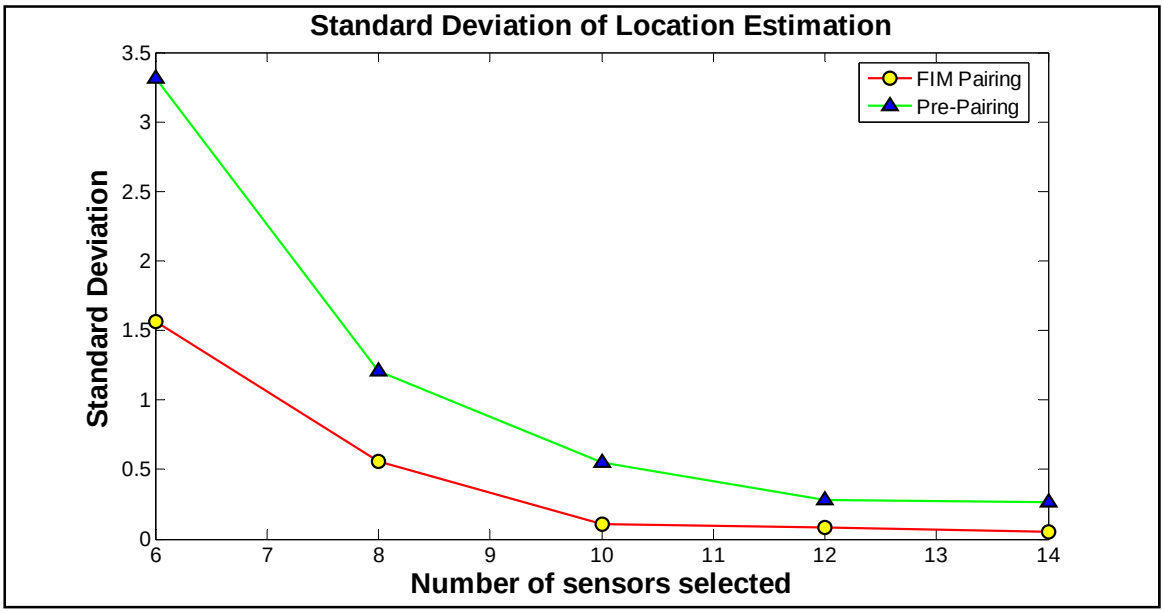

Figure 5 Performance of sensor selection w/o sharing

Figure 6 shows the time consumption used in pairing sensors for the non-sharing case versus the number of sensors/pairs selected. The upper line (-Δ-) shows the time required for the enumeration-based method, the lower one (-O-) shows the time required for our selection and pairing method. These time results are for Matlab-based implementations.

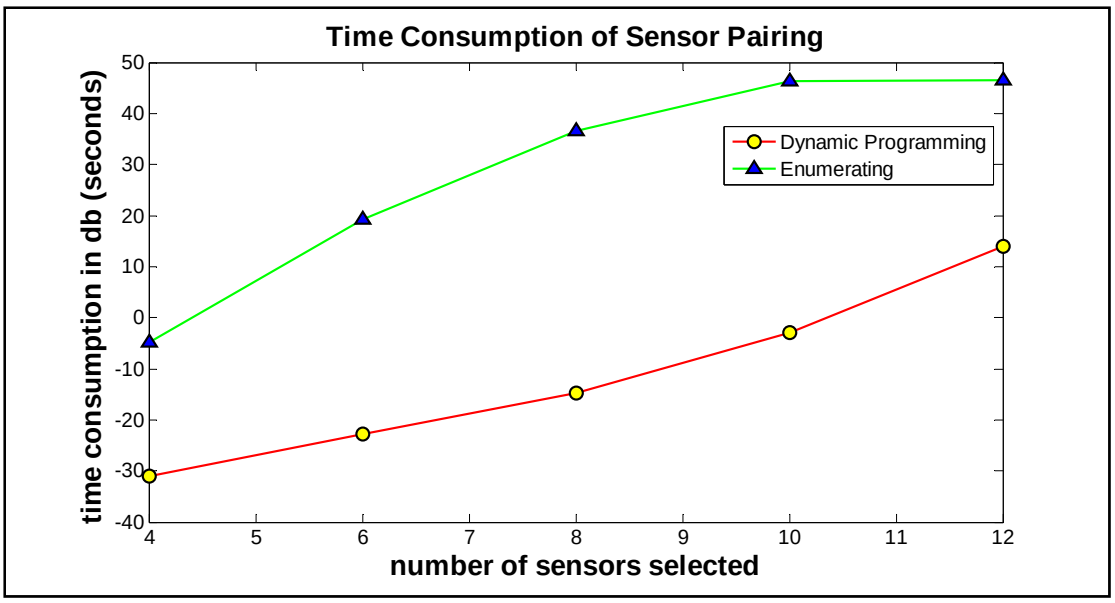

Figure 6 Time consumption of sensor pairing without sharing

Figure 7 shows the performance of sensor selections allowing sensor sharing. We select 5 to 11 sensors from 12, to make 4 to 10 pairs. It also shows the standard deviation of the geo-location error versus the number of sensors/pairs selected. The upper curve (-Δ-) shows the performance for the pre-paired sensor case with sharing; the lower curve (-O-) shows the performance using our selection and pairing method with sharing that is based on the Theorem in Section 3.2.

2.2.4 Discussion

The results above show that it is possible to select and pair an optimal subset of sensors while significantly retaining performance levels. The sensor selection optimization problem was based on the fact that the geometry property and data quality of sensors play important roles in the emitter location estimation. We have used Fisher information to capture this inter-play between data quality and geometry. We have discussed different situations: (i) pre-paired sensors vs. optimally pairing the sensors, and (ii) allowing shared sensors or not. Following are some general conclusions made from this work.

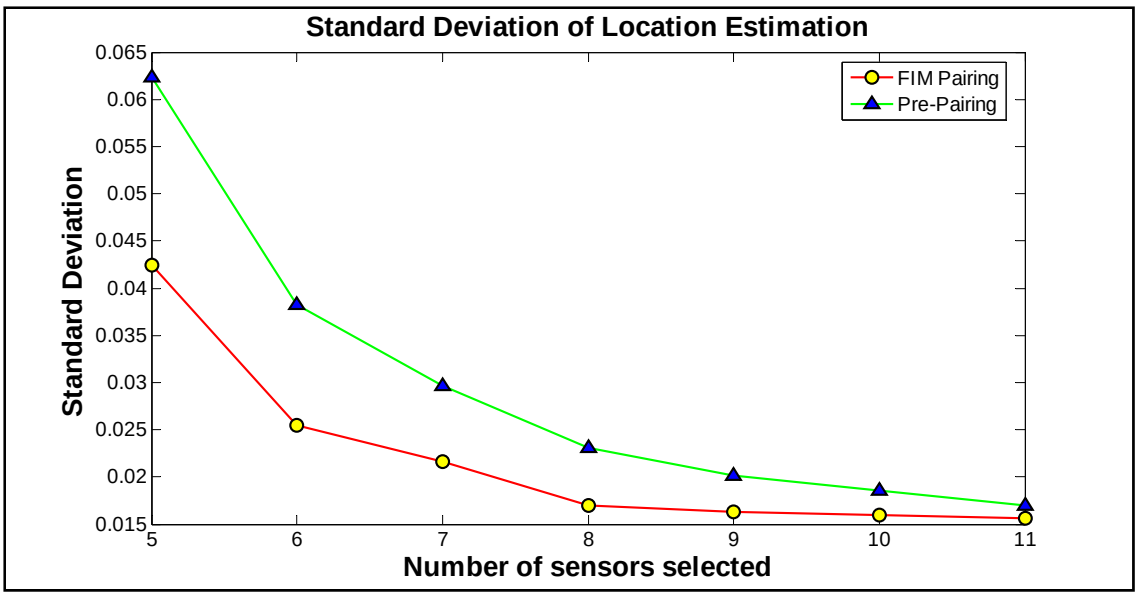

Figure 7 Performance of sensor selection allowed sharing

Conclusions: Without Sensor Sharing

- FIM of Geo-Location is easy to calculate, since each pair is independent;
- However, the pairing method is more complicated, since we need to consider all the possible pairing ways;
- From a system point of view, the communication among different pairs can be done simultaneously;
- The number of pairs needed is small; beyond a certain point the accuracy improves slowly as more pairs are selected to participate.

Conclusions: With Sensor Sharing

- For a total of N sensors we can have as many as $N-1$ pairs, the more the higher accuracy of location estimation;
- Fortunately, FIM of all the possible independent sets are the same, so we do not need to consider about the pairing method. One simple way is to pair the sensors in natural order. This is the main result of this work and leads to a major reduction in the optimization processing required.
- However, since not all the pairs are uncoupled, there are cross terms in the TDOA/FDOA FIM. This complicates the computation required to support the optimization processing.
- Some sensors work in more than one pair; the communication among them needs to be considered carefully to avoid collision. This will be the focus of future work.

2.2.5 Evaluation of FIM Cross-Term

Consider the case where two pairs share one sensor, as shown in Figure 8. The three received signals at the sensors are

$$\begin{aligned} s_1[n] &= s(nT-\tau_1)e^{jv_1 nT} + \omega_1[n] \\ s_2[n] &= s(nT-\tau_2)e^{jv_2 nT} + \omega_2[n] \\ s_3[n] &= s(nT-\tau_3)e^{jv_3 nT} + \omega_3[n] \end{aligned} \tag{20}$$

where $s(t)$ is the transmitted signal, and $\omega_i[n], i=1,2,3$ is the AWGN received by sensor.

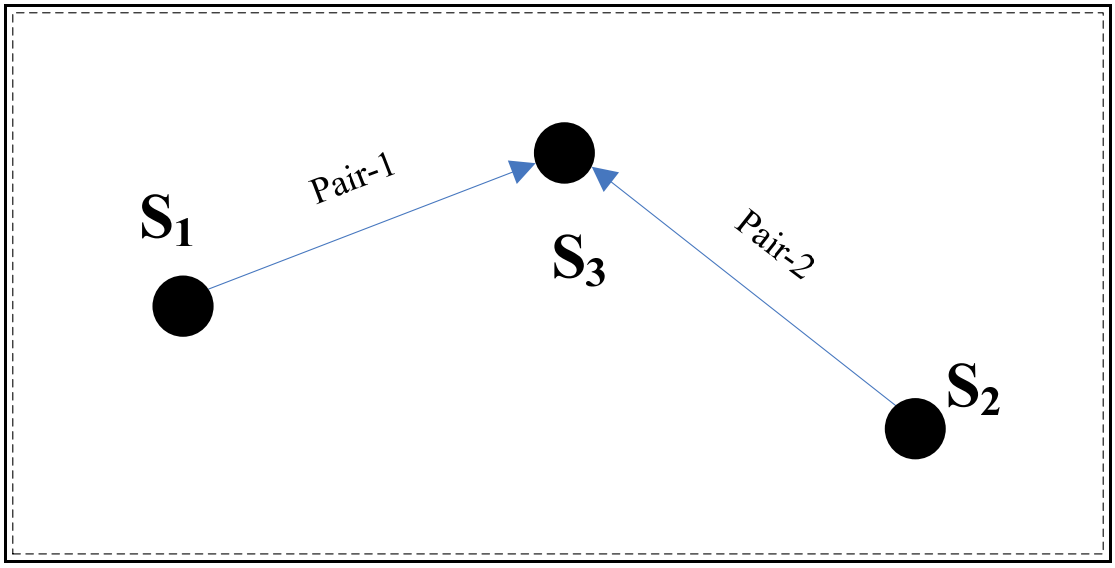

Figure 8 Two pairs shared one sensor

Let

$$\mathbf{s} = \begin{bmatrix} \mathbf{s}_1 \\ \mathbf{s}_2 \\ \mathbf{s}_3 \end{bmatrix} \quad and \quad \tau_{13} = \tau_1 - \tau_3; \quad \tau_{23} = \tau_2 - \tau_3 \tag{21}$$

The cross term FIM between pair-1 and pair-2 can be evaluated as

$$\mathbf{I}_{1,2}\Big|_{1,1} = \left(\frac{\partial \mathbf{s}}{\partial \tau_{1,3}}\right)^H \left(\frac{\partial \mathbf{s}}{\partial \tau_{2,3}}\right) \tag{22}$$

Since

$$\frac{\partial \mathbf{s}}{\partial \tau_{1,3}} = \begin{bmatrix} \frac{\partial \mathbf{s}_1}{\partial \tau_{1,3}} \\ \frac{\partial \mathbf{s}_2}{\partial \tau_{1,3}} \\ \frac{\partial \mathbf{s}_3}{\partial \tau_{1,3}} \end{bmatrix} = \begin{bmatrix} \frac{\partial \mathbf{s}_1}{\partial \tau_1} \cdot \frac{\partial \tau_1}{\partial \tau_{1,3}} \\ \mathbf{0} \\ \frac{\partial \mathbf{s}_3}{\partial \tau_3} \cdot \frac{\partial \tau_3}{\partial \tau_{1,3}} \end{bmatrix} = \begin{bmatrix} \frac{\partial \mathbf{s}_1}{\partial \tau_1} \\ \mathbf{0} \\ -\frac{\partial \mathbf{s}_3}{\partial \tau_3} \end{bmatrix} \tag{23}$$

also

$$\frac{\partial \mathbf{s}}{\partial \tau_{2,3}} = \begin{bmatrix} \frac{\partial \mathbf{s}_1}{\partial \tau_{2,3}} \\ \frac{\partial \mathbf{s}_2}{\partial \tau_{2,3}} \\ \frac{\partial \mathbf{s}_3}{\partial \tau_{2,3}} \end{bmatrix} = \begin{bmatrix} \mathbf{0} \\ \frac{\partial \mathbf{s}_2}{\partial \tau_2} \cdot \frac{\partial \tau_2}{\partial \tau_{2,3}} \\ \frac{\partial \mathbf{s}_3}{\partial \tau_3} \cdot \frac{\partial \tau_3}{\partial \tau_{2,3}} \end{bmatrix} = \begin{bmatrix} \mathbf{0} \\ \frac{\partial \mathbf{s}_2}{\partial \tau_2} \\ -\frac{\partial \mathbf{s}_3}{\partial \tau_3} \end{bmatrix} \tag{24}$$

Substitute (23) and (24) into (22), we get

$$\mathbf{I}_{1,1}^{(1,2)} = \left(\frac{\partial \mathbf{s}_3}{\partial \tau_3} \right)^H \left(\frac{\partial \mathbf{s}_3}{\partial \tau_3} \right) \tag{25}$$

This is exactly the FI of TDOA of sensor S_3's received signal. Following the same rule we get

$$\mathbf{I}_{1,2}\big|_{1,2} = \left(\frac{\partial \mathbf{s}}{\partial \tau_{1,3}} \right)^H \left(\frac{\partial \mathbf{s}}{\partial \nu_{2,3}} \right) = \left(\frac{\partial \mathbf{s}_3}{\partial \tau_3} \right)^H \left(\frac{\partial \mathbf{s}_3}{\partial \nu_3} \right) \tag{26}$$

$$\mathbf{I}_{1,2}\big|_{2,1} = \left(\frac{\partial \mathbf{s}}{\partial \upsilon_{1,3}} \right)^H \left(\frac{\partial \mathbf{s}}{\partial \tau_{2,3}} \right) = \left(\frac{\partial \mathbf{s}_3}{\partial \nu_3} \right)^H \left(\frac{\partial \mathbf{s}_3}{\partial \tau_3} \right) \tag{27}$$

$$\mathbf{I}_{1,2}\big|_{2,2} = \left(\frac{\partial \mathbf{s}}{\partial \nu_{1,3}} \right)^H \left(\frac{\partial \mathbf{s}}{\partial \nu_{2,3}} \right) = \left(\frac{\partial \mathbf{s}_3}{\partial \nu_3} \right)^H \left(\frac{\partial \mathbf{s}_3}{\partial \nu_3} \right) \tag{28}$$

Therefore the FIM cross-term between pairs is just the FIM of the shared sensor itself. The FIM of $\boldsymbol{\theta} = [\tau_{1,3}, \upsilon_{1,3}, \tau_{2,3}, \upsilon_{2,3}]^T$ is

$$\mathbf{J}(\boldsymbol{\theta}) = \begin{bmatrix} \mathbf{FI}_1 & \mathbf{I}_{1,2} \\ \mathbf{I}_{1,2} & \mathbf{FI}_2 \end{bmatrix} = \begin{bmatrix} \mathbf{F}_1 + \mathbf{F}_3 & \mathbf{F}_3 \\ \mathbf{F}_3 & \mathbf{F}_2 + \mathbf{F}_3 \end{bmatrix} \tag{29}$$

where $\mathbf{F}_i$ is the FIM of TDOA/FDOA of i^{th} sensor.

2.2.6 Example of Branch & Bound Used in Sensor Pairing

Branch and Bound method is a widely used algorithm for efficiently finding the optimal solution of an integer optimization problem. It is based on the fact that the enumeration of integer solutions has a tree structure. It begins "growing" the enumeration tree by creating partial solutions called "buds." The quality of a bud is assessed using the "bounding function," which provides an optimistic estimate of the best value that the objective function could possibly obtain by extending from a given bud. The best complete feasible solution found at any stage of growth of the tree is called the incumbent; a feasible solution is one that satisfies any given constraints. A complete solution occurs at a "leaf" in the tree. Efficiency is obtained by pruning unfruitful branches of the tree by using a "bounding function." Buds are pruned if (i) further growth can not yield a better result than the incumbent (i.e., the bounding function value of the bud is inferior to the objective function value of the incumbent), or (ii) further growth can not yield any feasible solutions. The optimal solution is found when further growth can not occur. For our application a feasible solution is one for which no sensor sharing occurs.

Consider an example of the sensor pairing and selection for $N = 8$ sensors; there are 28 possible pairs. In this example we will arbitrarily assign values for the each pair so as to illustrate the typical operation. Our objective function is

$$\max_{feasible\ solution} \left\{ \sum_{n=1}^{N/2} trace(FIM_{n^{th}\ pair\ in\ a\ solution}) \right\} \tag{30}$$

Here, feasible solution is the combination of sensor pair without sensor sharing. The bounding function used is

$$\max_{any\ solutions} \left\{ \sum_{n=1}^{N/2} trace(FIM_{n^{th}\ pair\ in\ a\ solution}) \right\} \tag{31}$$

The solution in bounding function can be any combination of sensors, shared or non-shared. Let (*n*, *m*) represent the pairing of sensor-*n* and sensor-*m*. In the first step, without loss of generality, we choose as buds that are the pairs that include sensor-1. Figure 9 shows this first layer of buds. If we choose pair (1,2) as the first pair, then the bounding function value for it is 71 in this example, which leaves pairs (3,5)-(3,6)-(7,8) as the subsequent possible pairs. Since sensor-1 and sensor-2 are actually paired, we did not reuse them in the bounding function calculation at this node or any descendent nodes. From the bounding function value we know that the very best objective function value that we might have at a leaf node descended from (1,2) is 71. Since sensor-3 is shared between two pairs, this solution is not feasible, but at this stage it is retained because this infeasible solution is simply used to evaluate the bounding function for the feasible solutions that lie below this bud.

The first step of the tree is generated from the root node by enumerating all the possible pairs which have sensor-1. By evaluating the bounding function, we get our first

incumbent (i.e., best feasible solution so far) as (1,5)-(2,4)-(3,6)-(7,8) , as incumbent=70; the buds that are shown exceeding this value can not be the incumbent because their bounding functions are computed based on infeasible solutions; however, they are retained to be grown further in hope that they may yield winning feasible solutions in the future. We now prune the pairs (1,6) and (1,8), because their bounding function values are smaller than the incumbent's.

Pruned nodes are indicated by a dashed border, the incumbent node is indicated by a bold solid border; nodes whose bounding function value is larger than the incumbent's but are based on infeasible solutions are shown by a non-bold solid border.

There needs to be a policy that governs the choice of the next bud for expansion; we use the global-best node selection policy, which chooses from all the bud nodes on the tree the one that has the best value of the bounding function. Thus, we choose pair (1,7) , which has the largest bounding function value, for first further expansion. This gives the next tree step as shown in Figure 10.

This expansion is generated from the (1,7) node by enumerating all the possible pairs which have sensor-2, this is based on the so-called natural order. After evaluating all the bounding function values, some new nodes were pruned. But a new incumbent was not found in this expansion. Also, the global-best node selection policy assesses the bounding function values of all current remaining nodes (even those in the "Step-1 layer"), and chooses the one with the best bounding function value to expand further. Thus, the partial solution (1,7)-(2,4) is expanded next, which gives the result shown in Figure 11.

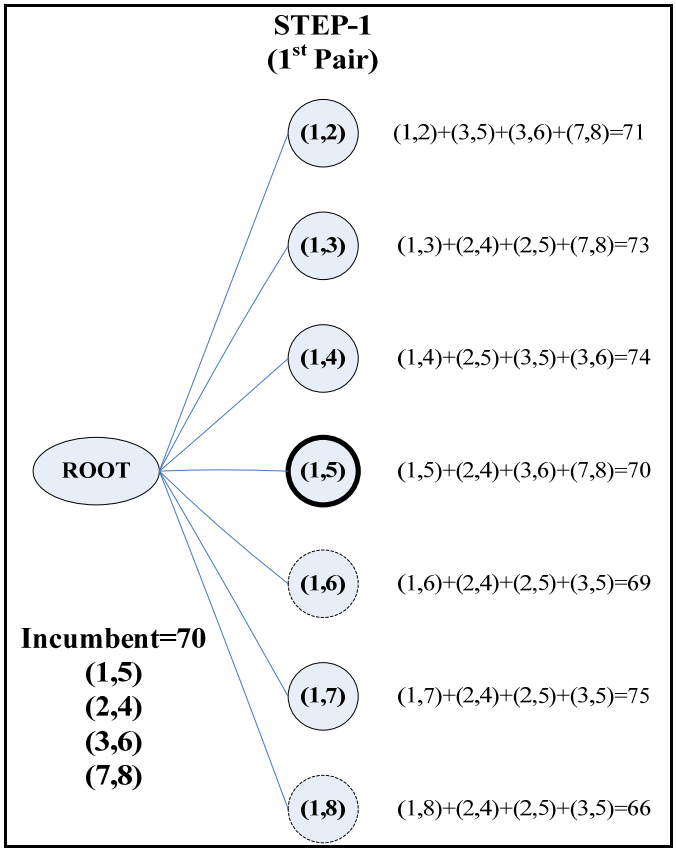

Figure 9: Illustration of first step of tree

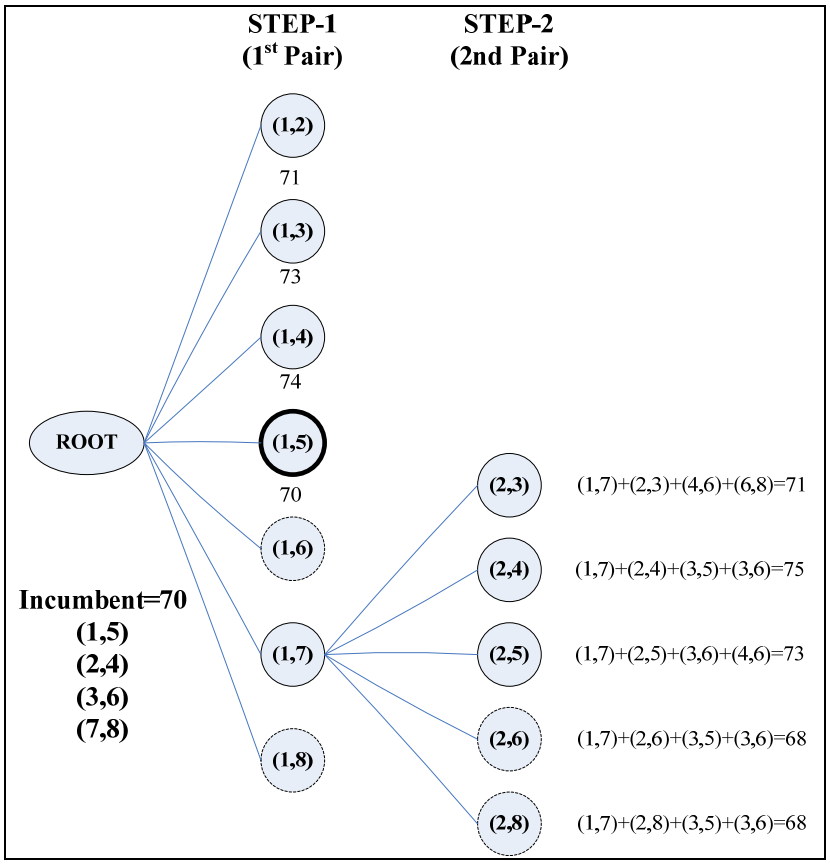

Figure 10: Illustration of second step in tree

We now have found that (1,7)-(2,4)-(3,5) is a feasible solution with a value higher than the previous incumbent's value of 70 and higher than any other feasible bud; thus, it becomes the incumbent with a value of 74. Note that now all other remaining buds have bounding function values that are less than or equal to the incumbent's value of 74; therefore, it is impossible for any of these buds to generate a feasible solution that beats the current incumbent. Thus, all other nodes are shown as pruned in Figure 11, and (1,7)-(2,4)-(3,5)-(6,8) is the optimal feasible solution It should be noted that if all the buds grown out of (2,4) had a bounding function value less than the incumbent in Figure 10, then they would all be pruned; then the global-best node selection rule would go back to (1,4) and grow from there because it has the largest bounding function value of all buds grown so far on whole tree.

In this particular example, we only evaluated 15 nodes, which is much smaller than the work of a full enumeration of the 105 possible solutions.

Simulation in Figure 12 gives the comparison of time consumption between enumeration method and the branch and bound method. We only let $N = 14$ for the largest number, since for larger N, the enumeration method is virtually impossible to realize.

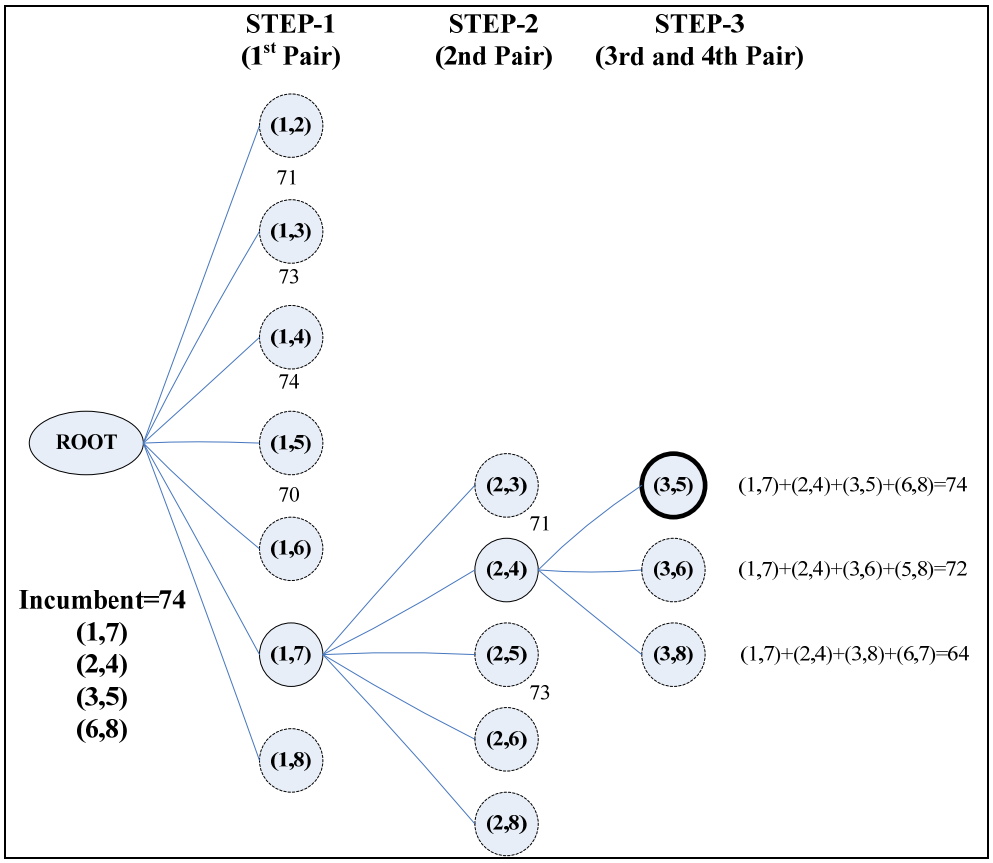

Figure 11: Illustration of third step in tree

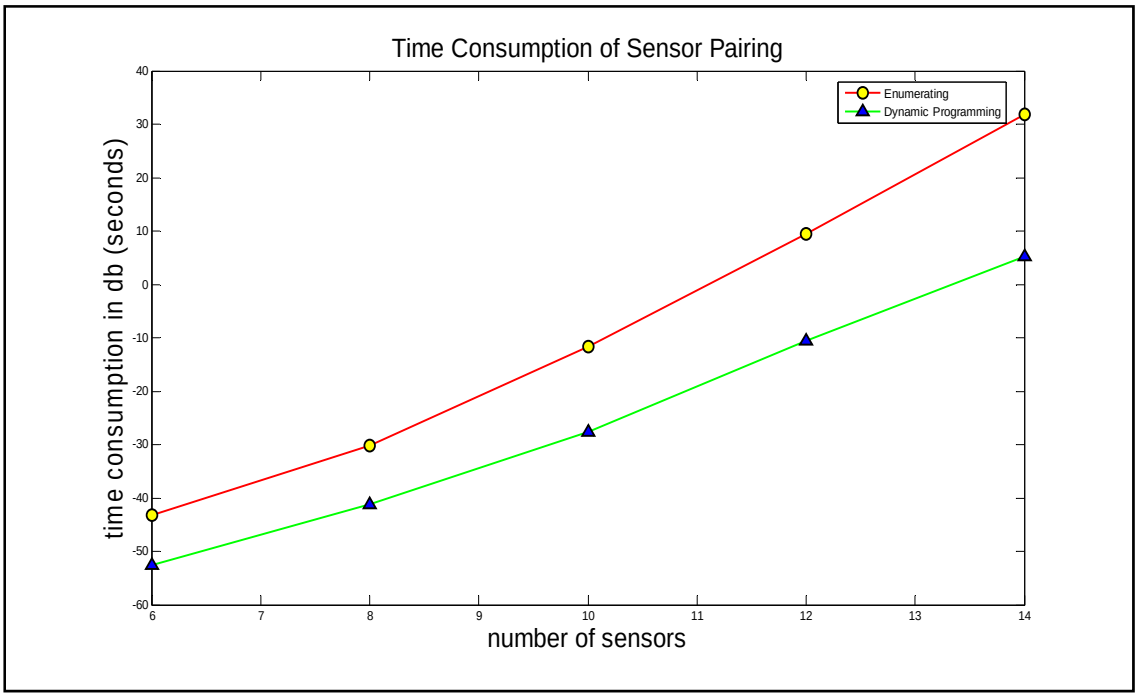

Figure 12 Time consumption of sensor pairing

2.2.7 Proof of Theorem

Let r_k be the distance between S_k and the emitter and let $r_{k,j} = r_k - r_j$ be the sensor-emitter distance difference for $k, j \in \{1,2,...N\}, k \neq j$. Then the relations between r_k and $r_{k,j}$ are as following

$$\begin{bmatrix} r_{k_1 j_1} \\ r_{k_2 j_2} \\ \vdots \\ r_{k_M j_M} \end{bmatrix}_{M\times 1} = \mathbf{T}_{M\times N} \begin{bmatrix} r_1 \\ r_2 \\ \vdots \\ r_N \end{bmatrix}_{N\times 1} = \mathbf{T}\cdot\mathbf{r} \tag{32}$$

where $\mathbf{T}$ is an $M \times N$ matrix, (M is the number of pairs and N is the number of sensors), which has only one '1' and one '-1' in each row. For the structure of $\mathbf{T}$, the rank of $\mathbf{T}$ is less than $N-1$, which means there are at most $N-1$ r_{kj} independent pairs. Independent pairs, simply speaking, means that there are no closed loops in the graph of the sensors in the subset. For example, in the pairing in Figure 13, the pairs (1,2), (1,3) and (2,3) are dependent pairs; (3,4), (4,5) and (5,6) are independent pairs.

Let there be a different reference sensor (RS) in each different independent set as in Figure 14. In set-I, S_i is the RS; in set-J, S_j is the RS.

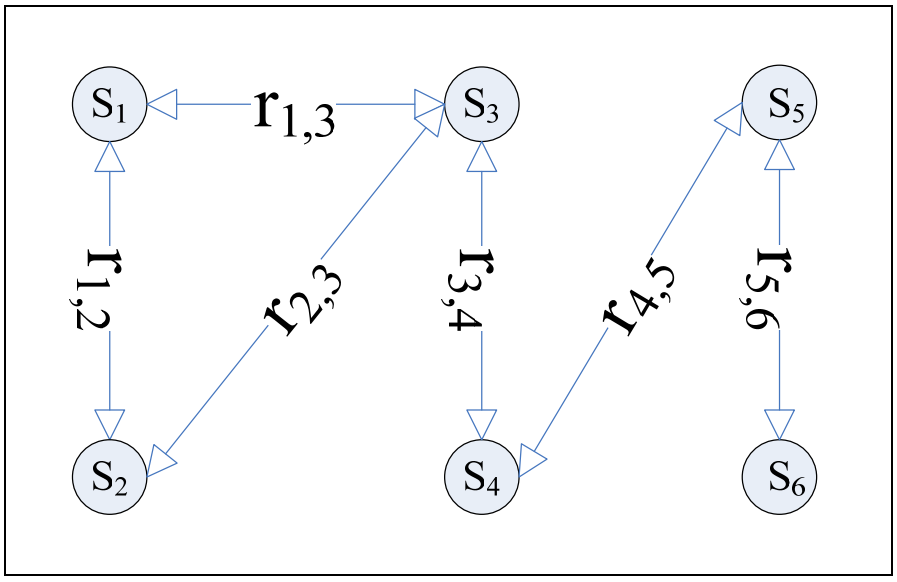

Figure 13 Independent and dependent pairs

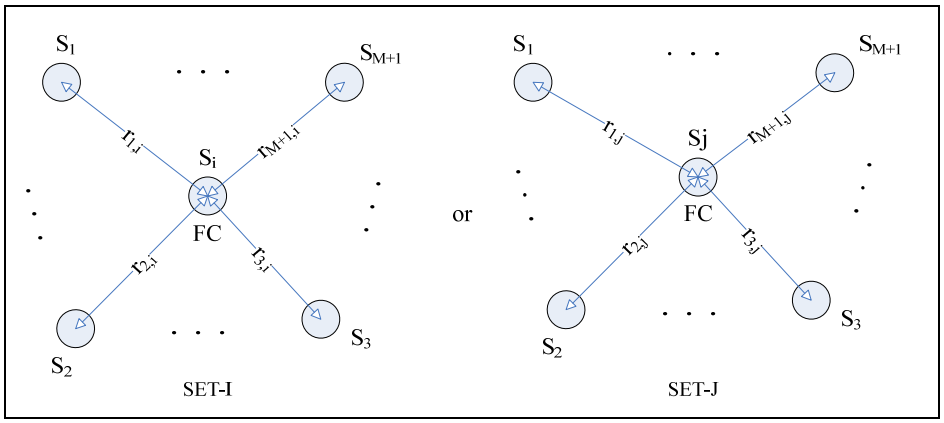

Figure 14 Same subset with different reference sensor

Let c be the signal propagation speed, the range difference equation is

$$r_{kj} = c\tau_{kj} = r_k - r_j \tag{33}$$

When the receivers are moving, taking time derivative of (33) yields a set of FDOA measurement equations

$$\dot{r}_{kj} = c\dot{\tau}_{kj} = \dot{r}_k - \dot{r}_j \tag{34}$$

where $\dot{r}_i$ is the rate of change of r_i. From the time derivative of (3), $\dot{r}_i$ is related to the unknown location $\mathbf{u}$ by

$$\dot{r}_i = \frac{(\mathbf{x}_i - \mathbf{u})^T \dot{\mathbf{x}}_i}{r_i} \tag{35}$$

Let $\mathbf{rd} = [r_1, r_2, \ldots, r_N, \dot{r}_1, \dot{r}_2, \ldots, \dot{r}_N]^T$, $\mathbf{p}_i = [r_{1i}, \ldots, r_{ki}, \ldots, r_{Ni}; \dot{r}_{1i}, \ldots, \dot{r}_{ki}, \ldots, \dot{r}_{Ni}]^T, k \neq i$ and $\mathbf{p}_j = [r_{1j}, \ldots, r_{kj}, \ldots, r_{Nj}; \dot{r}_{1j}, \ldots, \dot{r}_{kj}, \ldots, \dot{r}_{Nj}]^T, k \neq j$ then

$$\mathbf{p}_i = \begin{bmatrix} \mathbf{T}_i & \mathbf{0} \\ \mathbf{0} & \mathbf{T}_i \end{bmatrix} \mathbf{rd} = \mathbf{H}_i \mathbf{rd} \tag{36}$$

$$\mathbf{p}_j = \begin{bmatrix} \mathbf{T}_j & \mathbf{0} \\ \mathbf{0} & \mathbf{T}_j \end{bmatrix} \mathbf{rd} = \mathbf{H}_j \mathbf{rd} \tag{37}$$

where $\mathbf{T}_i$ and $\mathbf{T}_j$ are $(N-1)\times N$ matrixes, which only has one '1' and one '-1' in each row, and $\mathbf{0}$ is a $(N-1)\times N$ matrix with all 0 entries. It is easy to verify that there exists a $2(N-1)\times 2(N-1)$ full rank matrix $\mathbf{Q}_{ij}$, which satisfies

$$\mathbf{H}_j = \mathbf{Q}_{ij} \cdot \mathbf{H}_i \tag{38}$$

$$\mathbf{p}_j = \mathbf{H}_j \cdot \mathbf{rd} = \mathbf{Q}_{ij} \cdot \mathbf{H}_i \cdot \mathbf{rd} = \mathbf{Q}_{ij} \cdot \mathbf{p}_i \tag{39}$$

Then

$$\begin{aligned} CRLB(\hat{\mathbf{p}}_j) &= [\frac{\partial \mathbf{g}(\mathbf{p}_i)}{\partial \mathbf{p}_i}] \cdot CRLB(\hat{\mathbf{p}}_i) \cdot [\frac{\partial \mathbf{g}(\mathbf{p}_i)}{\partial \mathbf{p}_i}]^T \\ &= \mathbf{Q}_{ij} \cdot CRLB(\hat{\mathbf{p}}_i) \cdot \mathbf{Q}_{ij}^T \end{aligned} \tag{40}$$

Denote the emitter location $\mathbf{u}$ estimated by sensor pair set-I as $\hat{\mathbf{u}}_i$; then the CRLB of $\hat{\mathbf{u}}_i$ is

$$\text{CRLB}(\hat{\mathbf{u}}_i) = \mathbf{G}_i^T \cdot \mathbf{C}_i^{-1} \cdot \mathbf{G}_i \tag{41}$$

where $\mathbf{C}_i = E[\hat{\mathbf{p}}_i \cdot \hat{\mathbf{p}}_i^T]$ is the covariance matrix of the TDOA/FDOA estimates.
Since TDOA/FDOA are estimated by the ML method, we can assume that the covariance of the estimates achieve the CRLB, so $\mathbf{C}_i = CRLB(\hat{\mathbf{p}}_i)$ and

$$\mathbf{C}_j = CRLB(\hat{\mathbf{p}}_j) = \mathbf{Q}_{ij} \cdot CRLB(\hat{\mathbf{p}}_i) \cdot \mathbf{Q}_{ij}^T = \mathbf{Q}_{ij} \cdot \mathbf{C}_i \cdot \mathbf{Q}_{ij}^T \tag{42}$$

where $\mathbf{G}_i$ is the Jacobin matrix of set-I defined by

$$\mathbf{G}_j = \frac{\partial \mathbf{p}_j(\mathbf{u})}{\partial \mathbf{u}} = \frac{\partial}{\partial \mathbf{u}}[\mathbf{Q}_{ij} \cdot \mathbf{p}_i(\mathbf{u})] = \mathbf{Q}_{ij} \cdot \frac{\partial \mathbf{p}_i(\mathbf{u})}{\partial \mathbf{u}} = \mathbf{Q}_{ij} \cdot \mathbf{G}_i \tag{43}$$

Then

$$\begin{aligned} \text{CRLB}(\hat{\mathbf{u}}_j) &= \mathbf{G}_j^T \cdot \mathbf{C}_j^{-1} \cdot \mathbf{G}_j \\ &= (\mathbf{Q}_{ij} \cdot \mathbf{G}_i)^T \cdot (\mathbf{Q}_{ij} \cdot \mathbf{C}_i \cdot \mathbf{Q}_{ij}^T)^{-1} \cdot (\mathbf{Q}_{ij} \cdot \mathbf{G}_i) \\ &= \mathbf{G}_i^T \cdot [\mathbf{Q}_{ij}^T (\mathbf{Q}_{ij}^T)^{-1}] \cdot \mathbf{C}_i^{-1} \cdot [\mathbf{Q}_{ij}^{-1} \mathbf{Q}_{ij}] \cdot \mathbf{G}_i \\ &= \mathbf{G}_i^T \cdot \mathbf{C}_i^{-1} \cdot \mathbf{G}_i \\ &= \text{CRLB}(\hat{\mathbf{u}}_i) \end{aligned} \tag{44}$$

Thus, we have proved that for all the independent sets, the CRLB of emitter location estimation are the same.

3 Refinement & Extension of Previous Results

3.1 Improved Geometry-Adaptive Compression

Code was written for this but never successfully made to run. The effort was re-directed to the Sensor Selection Task, which proved to be harder than anticipated.

3.2 Using the STFT

Code was developed and successfully tested. The code is included in the Matlab code delivered separately from this report Surprisingly the resulting performance was not much different than when using the orthogonal wavelet-packet filter bank despite the fact that it has been shown to be better at estimating the Fisher information.

4 Integration into a Matlab-based Test-Bed

Code for a Matlab testbed has been developed for testing the compression methods developed at Binghamton University. The code will be delivered separately from this report.

5 General Location Studies

5.1 Develop & Offer Short Course

Course notes are complete although there are new issues for which new notes could and will be developed outside the support of this grant. Plans to offer the lectures were attempted twice (to offer in January 2007, to offer in June 2007) but both plans were aborted due to challenges in schedules. As a way to satisfy this task, video lectures are under production and will be provided to AFRL at a later date to be determined – terms of use for these video lectures are currently under discussion with AFRL personnel.

5.2 Concept Studies, Evaluation, and Analysis

During the discussions at status meetings it became clear that AFRL researchers were consulting many of the early papers on TDOA/FDOA that were written by sonar researchers. The PI was concerned that these sonar-based results may not be directly applicable to TDOA/FDOA for electromagnetic communication signals. As part of this funded effort, it has been discovered that many widely-known results in the TDOA/FDOA literature are not at all applicable to the case when the signals are

electromagnetic signals. That is, results that have been developed under the assumption that the signal is a WSS Gaussian process (the preferred model for many of the early sonar-driven papers on TDOA/FDOA) may not carry over to the electromagnetic case, which is not accurately modeled by a WSS Gaussian process. The PI has developed modified results for many of the early (sonar-based) TDOA/FDOA results to extend them to the electromagnetic case.

The location of a source can be determined from signals intercepted at several sensors. One of the most effective methods is to use estimates of the time-difference-of-arrival (TDOA) and/or the frequency-difference-of-arrival (FDOA) between pairs of signals received at the sensors. This involves a sequence of two estimation problems: (i) processing the signals to give a set of TDOA/FDOA estimates (e.g., [3], [5], [6], [7], [8], [9], [10], [12], [14], [15], [16]), and (ii) processing the resulting TDOA/FDOA estimates to estimate the location (e.g., [4], [11], [13]).

Optimal processing for the second stage requires an understanding of the probabilistic characteristics of the TDOA/FDOA estimates from the first stage. Therefore, much work has been done to derive optimal TDOA/FDOA estimates and to characterize their covariance matrix. However, as this correspondence will point out, when using results from the many papers on TDOA/FDOA estimation it is important to understand the differences that arise due to the different signal models that have been used. TDOA/FDOA results were first developed in the early 1970s for the case of passively locating underwater acoustic sources, where the accepted model for the signal is a WSS random process (almost always assumed Gaussian) [3], [5], [6], [7], [8], [10], [12], [14]. Only later was TDOA/FDOA-based location considered for the case of passively locating electromagnetic sources [9], [11], [13], [16]. For electromagnetic sources such as radar and communication transmitters, a stationary random process is generally deemed inappropriate and a deterministic signal model may be better [16]. Stein [16] considers the development of the ML estimator for the deterministic case (but did not develop the Cramer-Rao bound for that case) and Quazi [8] briefly addresses the deterministic vs. random signal differences but only in the context between active vs. passive location systems (he does not mention differences between passive systems for the acoustic and electromagnetic scenarios). In general, there seems to be confusion and unawareness about the differences between the passive acoustic case and the passive electromagnetic case[2]. For example, many times acoustic-signal results have been misused in the electromagnetic scenario; this seems to occur more often than the reverse –likely due to the fact that the acoustic setting was the first explored and has generated many widely-known publications.

5.2.1 Impact of Signal Model on TDOA/FDOA Results

5.2.1.1 Signal Models

The model for two sampled passively-received complex baseband signals at two sensors is given by

[2] We use the terms "acoustic" and "electromagnetic" as merely convenient labels that arise from the historical development of TDOA/FDOA results; it *is* of course *possible* to have an acoustic signal that is better modeled as deterministic or to have an electromagnetic signal better modeled as random.

$$r_1[n] = s(nT - \tau_1)e^{j\nu_1 nT} + w_1[n]$$
$$r_2[n] = s(nT - \tau_2)e^{j\nu_2 nT} + w_2[n] \tag{45}$$

where $s(t)$ is the complex envelope of the continuous-time transmitted signal, T is the sampling interval, the $w_i[n]$ are corrupting noises, τ_1 and τ_2 are delays, and ν_1 and ν_2 are Doppler shifts. It should be mentioned that for electromagnetic signals it is usually appropriate to use Doppler *shift* to model the effect of motion between source and receiver, but for acoustic signals it is often not appropriate to use Doppler *shift*; however, to allow easier focus on the statistical model differences we assume here that this is valid. The TDOA $\Delta_\tau = \tau_1 - \tau_2$ and the FDOA $\Delta_\nu = \nu_1 - \nu_2$ are the parameters to be estimated from time-domain samples of these signals; we define $\boldsymbol{\theta} = \begin{bmatrix} \Delta_\tau & \Delta_\nu \end{bmatrix}^T$. For both the acoustic scenario and the electromagnetic scenario, the accepted modeling assumptions for the noises $w_i[n]$ are (i) they are zero-mean WSS random processes, (ii) they are each Gaussian, and (iii) they are independent of each other. In general they are not necessarily assumed to be white, but that is a common assumption. For notational purposes: (i) the signal $s_i[n] = s(nT - \tau_i)e^{j\nu_i nT}$, (ii) the vector $\mathbf{r}_i$ is the vector with elements that are the values of $r_i[n]$, and (iii) the vector $\mathbf{r}$ is $\mathbf{r} = \begin{bmatrix} \mathbf{r}_1^T & \mathbf{r}_2^T \end{bmatrix}^T$; the vector $\mathbf{s}$ is defined as $\mathbf{s}_{\boldsymbol{\theta}} = \begin{bmatrix} \mathbf{s}_1^T & \mathbf{s}_2^T \end{bmatrix}^T$, where we explicitly notate the dependence on the TDOA/FDOA parameter vector $\boldsymbol{\theta}$.

This much is common between the acoustic and electromagnetic scenarios. The differences arise in what is assumed about the signal $s_i[n]$. For the acoustic scenario the accepted modeling assumptions on the signal $s_i[n]$ are: (i) it is a zero-mean WSS random process, (ii) it is Gaussian, (iii) it is independent of each noise process, and (iv) it need not be assumed white, although that is a special case that is often considered. This random-signal model arose due to the fact that the early TDOA/FDOA researchers were investigating passive sonar, where the acoustic signals were made by the motors of ocean vehicles. For this scenario: (i) the WSS random process assumption is consistent with the erratic nature of the motor sounds, (ii) the Gaussian assumption is motivated by (perhaps) the central limit theorem and (certainly) the tractability it provides, and (iii) the independence of signal and the noises is reasonable based on physical considerations.

There are very few published fundamental results on TDOA/FDOA estimation for electromagnetic signals (e.g., [9], [16]). Signals emitted by electromagnetic sources tend to have much more regular structure than the erratic variations seen in acoustic signals made by ocean vehicles; therefore they don't readily evoke the notion of random process. Still, a classic example of a WSS random process is a sinusoidal signal with uniformly distributed phase; despite the fact that each realization of this process exhibits very regular structure it *is* a WSS random process. Similarly, radar pulse trains can be viewed as random processes for the very same reason: they can be modeled as having random transmission parameters (e.g., random time offset, random phase offset, etc.). However, such signals – with their widely spaced pulses – can hardly be thought to be WSS processes (e.g., variance within a pulse is not equal to the variance between pulses). Furthermore, they certainly cannot be modeled as Gaussian, and finding some other suitable probability model seems daunting and is generally fruitless when one tries to solve problems using such a probability model. Similar arguments could be made for

many other types of electromagnetic transmitted signals, though not for all. Thus, in such a scenario it is prudent to consider the signal $s_i[n]$ to be a deterministic signal rather than a random signal [16].

When we consider the estimates of TDOA and FDOA, $\hat{\Delta}_\tau$ and $\hat{\Delta}_v$, we typically wish to find unbiased estimates that minimize $E\left\{\left(\hat{\Delta}_\tau - \Delta_\tau\right)^2\right\}$ and $E\left\{\left(\hat{\Delta}_v - \Delta_v\right)^2\right\}$. Here is an immediate fundamental distinction between these two models: it needs to be understood that when the signal is random these expectations are taken over the combined ensemble of signal and noise whereas when the signal is deterministic these expectations are taken over only the noise ensemble. Thus, when the signal is random we are finding the average squared error over all possible noises *and* signals (within the ensemble); when the signal is deterministic we are finding the average squared error over all possible noises for *one specific* signal. Furthermore, in simulations for the random signal case, in each Monte Carlo run the signal is selected from its ensemble and the noise is selected from its ensemble; whereas for the deterministic signal case the same signal is used in every Monte Carlo run.

5.2.1.2 PDFs Under the Signal Models

Despite these differences, from the above discussion we see that for both models the received data vector $\mathbf{r}$ is Gaussian and has a Gaussian PDF. The key distinction between these two scenarios that drives all the differences in the FIM, the CRB, and the MLE processing is the manner in which the TDOA/FDOA impacts the parameters of the Gaussian PDF of data vector $\mathbf{r}$. For the case of the acoustic scenario, the mean of $\mathbf{r}$ is zero and the covariance matrix of $\mathbf{r}$ depends on TDOA/FDOA, so we denote it as $\mathbf{C}_{\boldsymbol{\theta}}$ to show that dependence. In contrast, for the case of the electromagnetic scenario, the mean of $\mathbf{r}$ is $\mathbf{s}_{\boldsymbol{\theta}} = \left[\mathbf{s}_1^T \quad \mathbf{s}_2^T\right]^T$ which depends on TDOA/FDOA and the covariance matrix of $\mathbf{r}$ is a block diagonal matrix of the two individual noise covariance matrices, and therefore does not depend on TDOA/FDOA so we denote it as $\mathbf{C}$ in this case. From this single distinction we see that the PDF for the acoustic case is

$$p_{ac}(\mathbf{r};\boldsymbol{\theta}) = \frac{1}{\det\left(\pi\mathbf{C}_{\boldsymbol{\theta}}\right)}\exp\left\{-\mathbf{r}^H\mathbf{C}_{\boldsymbol{\theta}}^{-1}\mathbf{r}\right\} \tag{46}$$

and the PDF for the electromagnetic case is

$$p_{em}(\mathbf{r};\boldsymbol{\theta}) = \frac{1}{\det\left(\pi\mathbf{C}\right)}\exp\left\{-(\mathbf{r}-\mathbf{s}_{\boldsymbol{\theta}})^H\mathbf{C}^{-1}(\mathbf{r}-\mathbf{s}_{\boldsymbol{\theta}})\right\}. \tag{47}$$

The differences between the PDFs for these two signal model scenarios is clearly evident in (46) and (47); it is this difference that leads to significant differences in the structures of Cramer-Rao bounds as well as the maximum likelihood estimators for the two cases. It should be observed that these are each a special case of the complex general Gaussian case (see Ch. 15 of [17] for the complex data case covered here) given by

$$p_{gg}(\mathbf{r};\boldsymbol{\theta}) = \frac{1}{\det\left(\pi \mathbf{C}_{\boldsymbol{\theta}}\right)} \exp\left\{-(\mathbf{r}-\boldsymbol{\mu}_{\boldsymbol{\theta}})^H \mathbf{C}_{\boldsymbol{\theta}}^{-1}(\mathbf{r}-\boldsymbol{\mu}_{\boldsymbol{\theta}})\right\}. \tag{48}$$

where both the mean $\boldsymbol{\mu}_{\boldsymbol{\theta}}$ and the covariance $\mathbf{C}_{\boldsymbol{\theta}}$ of $\mathbf{r}$ depend on the parameter vector $\boldsymbol{\theta}$.

5.2.1.3 Fisher Information and Cramer-Rao Bound

The elements of the Fisher information matrix $\mathbf{J}_{gg}$ for the complex general Gaussian scenario PDF in (48) is a standard result [17] given by

$$[J_{gg}]_{ij} = 2\,\mathrm{Re}\left(\left[\frac{\partial \boldsymbol{\mu}_{\boldsymbol{\theta}}}{\partial \theta_i}\right]^H \mathbf{C}^{-1}(\boldsymbol{\theta}) \left[\frac{\partial \boldsymbol{\mu}_{\boldsymbol{\theta}}}{\partial \theta_j}\right]\right) + \mathrm{tr}\left(\mathbf{C}_{\boldsymbol{\theta}}^{-1} \frac{\partial \mathbf{C}_{\boldsymbol{\theta}}}{\partial \theta_i} \mathbf{C}_{\boldsymbol{\theta}}^{-1} \frac{\partial \mathbf{C}_{\boldsymbol{\theta}}}{\partial \theta_j}\right). \tag{49}$$

Notice that there are two terms in this result: one that depends on the sensitivity of the *mean* to the parameters and one that depends on the sensitivity of the *covariance* to the parameters. Because the acoustic and electromagnetic scenarios are two different special cases of the generalized Gaussian scenario, we can use the result in (49) to find the result for each of these two special cases.

As discussed above, for the acoustic scenario the mean of $\mathbf{r}$ is zero and therefore does not depend on the parameter vector; thus the first term in (49) is zero and the Fisher information matrix $\mathbf{J}_{ac}$ for the acoustic scenario is then given by

$$\left[\mathbf{J}_{ac}\right]_{ij} = \mathrm{tr}\left[\mathbf{C}_{\boldsymbol{\theta}}^{-1} \frac{\partial \mathbf{C}_{\boldsymbol{\theta}}}{\partial \theta_i} \mathbf{C}_{\boldsymbol{\theta}}^{-1} \frac{\partial \mathbf{C}_{\boldsymbol{\theta}}}{\partial \theta_j}\right], \tag{50}$$

which gives a result that is well known in the TDOA/FDOA literature for the acoustic signal scenario (e.g., [10], [12]). The corresponding CRBs are found by inverting the respective FIM; doing that directly is difficult but equivalent approaches that avoid direct use of (50) have been found (see for example [12]).

For the electromagnetic scenario the covariance of $\mathbf{r}$ doesn't depend on the parameter vector; thus, the second term in (49) is zero and the Fisher information matrix $\mathbf{J}_{em}$ for the electromagnetic scenario is thus given by

$$\left[\mathbf{J}_{em}\right]_{ij} = 2\,\mathrm{Re}\left\{\frac{\partial \mathbf{s}_{\boldsymbol{\theta}}^H}{\partial \theta_i} \mathbf{C}^{-1} \frac{\partial \mathbf{s}_{\boldsymbol{\theta}}}{\partial \theta_j}\right\}, \tag{51}$$

which surprisingly is not widely seen in the TDOA/FDOA literature for the electromagnetic signal scenario. See Section 5.2.4 for details of evaluating this form to compute the FIM for TDOA/FDOA under the deterministic signal case. The corresponding CRBs are found by inverting the respective FIM; doing that using (51) leads to forms that are similar but not identical to those given without proof in [9] for the continuous-time case.

Comparing (50) and (51) we see that there is a significant difference between the structures of the FIM for the two cases. In particular, for the acoustic scenario it is convenient to use "Whittle's Theorem" to write the Fisher information for a WSS process in the spectral domain [14]; however, this alternative approach for the WSS-signal case can not be used for the electromagnetic scenario. An even more important distinction is as follows. As pointed out in several publications (e.g., [10], [12], [14]) the off-diagonal elements of the acoustic scenario FIM in (50) are zero under the mild assumption of a large time-bandwidth product, thus indicating that for the acoustic scenario the optimal estimate of TDOA should be uncorrelated with the optimal estimate of FDOA. However, the electromagnetic scenario FIM in (51) does not, in general, yield this uncorrelated TDOA/FDOA condition. For example, Section 5.2.4 shows that for the case of white noise the result in (51) gives the off-diagonal FI element as

$$[\mathbf{J}_{em}]_{12} = 2\,\mathrm{Re}\left\{\frac{1}{\sigma_1^2}\sum_n -jnTs^*(nT-\tau_1)s'(nT-\tau_1) + \frac{1}{\sigma_2^2}\sum_n -jnTs^*(nT-\tau_2)s'(nT-\tau_2)\right\}, \quad (52)$$

where $s'(t)$ is the derivative of $s(t)$. From this result we see that the off-diagonal element in general is not zero; as an illustration, the linear chirp signal has been shown to have non-zero cross-FI [18]. Thus, for the acoustic case we can expect that for a pair of sensors the optimal TDOA estimate is uncorrelated from the optimal FDOA estimate but that should not be expected in the electromagnetic case.

An important impact of this comes when assessing the location accuracy that can be achieved from a set of TDOA/FDOA measurements. Assuming an ML estimator for the TDOA/FDOA values, their estimates can be taken to be Gaussian and then the CRB on the location estimate covariance becomes

$$\mathbf{C}_{loc} = (\mathbf{G}^T\mathbf{J}\mathbf{G})^{-1} \quad (53)$$

where $\mathbf{J}$ is the FIM for all N TDOA/FDOA measurements and $\mathbf{G}$ is the Jacobian of the TDOA/FDOA values with respect to the emitter's location coordinates [13], [19]. From (53) it is clear that when performing studies of location accuracy, using the incorrect FIM for TDOA/FDOA – i.e., using the acoustic FIM when the electromagnetic FIM should be used, or vice versa – can lead to incorrect conclusions about location accuracy.

5.2.1.4 Maximum Likelihood Estimator

The ML estimator is found by maximizing the log likelihood function (LLF), which is typically expressed by taking partial derivatives of the LLF with respect to each parameter and setting them equal to zero. For the complex generalized Gaussian case there is a standard result (see Sect. 15.7 of [17]) given by

$$\frac{\partial \ln\{p_{gg}(\mathbf{r};\boldsymbol{\theta})\}}{\partial\theta_i} = -\mathrm{tr}\left(\mathbf{C}_{\boldsymbol{\theta}}^{-1}\frac{\partial\mathbf{C}_{\boldsymbol{\theta}}}{\partial\theta_i}\right) + 2\,\mathrm{Re}\left\{[\mathbf{r}-\boldsymbol{\mu}_{\boldsymbol{\theta}}]^H\mathbf{C}_{\boldsymbol{\theta}}^{-1}\frac{\partial\boldsymbol{\mu}_{\boldsymbol{\theta}}}{\partial\theta_i}\right\} + [\mathbf{r}-\boldsymbol{\mu}_{\boldsymbol{\theta}}]^H\mathbf{C}_{\boldsymbol{\theta}}^{-1}\frac{\partial\mathbf{C}_{\boldsymbol{\theta}}}{\partial\theta_i}\mathbf{C}_{\boldsymbol{\theta}}^{-1}[\mathbf{r}-\boldsymbol{\mu}_{\boldsymbol{\theta}}]. \quad (54)$$

Notice that there are three terms in this result: one that depends on the sensitivity of the mean to the parameters and two that depend on the sensitivity of the covariance to the parameters. Because the acoustic and electromagnetic scenarios are two different special cases of the generalized Gaussian scenario, we can use the result in (54) to find the result for each of these two special cases.

For the acoustic scenario the mean of $\mathbf{r}$ is zero and therefore does not depend on the parameter vector; thus, the partial derivatives of the LLF for (46) are given by just two terms from (54):

$$\begin{aligned}\frac{\partial p_{ac}(\mathbf{r};\boldsymbol{\theta})}{\partial \theta_i} &= -\frac{\partial}{\partial \theta_i}\ln\left[\det\left(\pi\mathbf{C}_{\boldsymbol{\theta}}\right)\right] - \frac{\partial}{\partial \theta_i}\mathbf{r}^H\mathbf{C}_{\boldsymbol{\theta}}^{-1}\mathbf{r} \\ &= -\operatorname{tr}\left(\mathbf{C}_{\boldsymbol{\theta}}^{-1}\frac{\partial \mathbf{C}_{\boldsymbol{\theta}}}{\partial \theta_i}\right) + \mathbf{r}^H\mathbf{C}_{\boldsymbol{\theta}}^{-1}\frac{\partial \mathbf{C}_{\boldsymbol{\theta}}}{\partial \theta_i}\mathbf{C}_{\boldsymbol{\theta}}^{-1}\mathbf{r}\end{aligned} \tag{55}$$

This result is well known in the passive sonar literature (e.g., see [10],[12]). In [12] it is further stated that for the TDOA/FDOA case the determinant term in the first line of (55) does not depend on the parameter vector; therefore, the first term in the second line of (55) can be ignored to give

$$\frac{\partial p_{ac}(\mathbf{r};\boldsymbol{\theta})}{\partial \theta_i} = \mathbf{r}^H\mathbf{C}_{\boldsymbol{\theta}}^{-1}\frac{\partial \mathbf{C}_{\boldsymbol{\theta}}}{\partial \theta_i}\mathbf{C}_{\boldsymbol{\theta}}^{-1}\mathbf{r}\,. \tag{56}$$

It should be noted that finding the value of θ that drives (56) to zero is equivalent to

$$\hat{\boldsymbol{\theta}}_{ML,ac} = \arg\max_{\boldsymbol{\theta}}\left\{-\mathbf{r}^H\mathbf{C}_{\boldsymbol{\theta}}^{-1}\mathbf{r}\right\} \tag{57}$$

For the electromagnetic scenario the covariance of $\mathbf{r}$ does not depend on the parameter vector; thus, the partial derivatives of the LLF for (47) are given by the second term in (54)

$$\frac{\partial p_{em}(\mathbf{r};\boldsymbol{\theta})}{\partial \theta_i} = 2\operatorname{Re}\left\{\left[\mathbf{r}-\mathbf{s}_{\boldsymbol{\theta}}\right]^H\mathbf{C}^{-1}\frac{\partial \mathbf{s}_{\boldsymbol{\theta}}}{\partial \theta_i}\right\}. \tag{58}$$

It should be noted that finding the value of $\boldsymbol{\theta}$ that drives (58) to zero is equivalent to

$$\begin{aligned}\hat{\boldsymbol{\theta}}_{ML,em} &= \arg\max_{\boldsymbol{\theta}}\left\{-[\mathbf{r}-\mathbf{s}_{\boldsymbol{\theta}}]^H\mathbf{C}^{-1}[\mathbf{r}-\mathbf{s}_{\boldsymbol{\theta}}]\right\} \\ &= \arg\max_{\boldsymbol{\theta}}\left\{2\operatorname{Re}\left\{\mathbf{r}^H\mathbf{C}^{-1}\mathbf{s}_{\boldsymbol{\theta}}\right\} - \mathbf{s}_{\boldsymbol{\theta}}^H\mathbf{C}^{-1}\mathbf{s}_{\boldsymbol{\theta}}\right\}\end{aligned} \tag{59}$$

Comparing (56) and (57) to (58) and (59) shows that we should expect fundamental differences between the MLE for the acoustic and electromagnetic cases. Surprisingly though, each case results in a structure that involves pre-filtering the received signals followed by cross-correlation (see [5], [12] for the acoustic case and [16] for the

electromagnetic case). However, although both cases share this generalized correlator structure, the pre-filtering needed for each case is quite different. For the acoustic case the filters depend on an interplay between the signal PSD and the noise PSD [5], [12], whereas for the electromagnetic case the filters depend only on the noise PSD and not on the signal's spectral structure [16]. As a result, the acoustic generalized correlator simplifies to a standard correlator only when noise and signal are white [5], [7] whereas the electromagnetic generalized correlator simplifies to a standard correlator whenever the noise is white, regardless of the signal's spectral structure [16]. Despite this difference in ML structure for the two scenarios there are many cases in the literature that address the electromagnetic case but reference (and sometimes use) the acoustic scenario's generalized correlator when it is not appropriate.

Another interesting difference between the two scenarios is pointed out by Stein [16]. For the deterministic signal, the MLE involves estimating the unknown deterministic signal. It is clear from (59) that this step is necessary since the maximization in (59) involves the *unknown* signal vector $\mathbf{s}_{\boldsymbol{\theta}}$. The development of the MLE for this scenario naturally includes the estimation of the underlying signal as an *intrinsic* part of the processing.

Weinstein [10] explored the losses that arise when the ML estimator for TDOA/FDOA is done on a decentralized pairwise basis rather than using all received signals in a centralized processor to jointly estimate all TDOA/FDOA values. Although Weinstein does not explicitly state that he considers only the passive acoustic scenario nor does he state that the signal is modeled as a WSS Gaussian process, the PDF that he uses is given by (46) and not by (47) and therefore all the results in [10] are applicable to the acoustic scenario but not to the electromagnetic scenario. It is not clear that Weinstein's general insights for the near equivalence of decentralized and centralized processing when the SNR is high carries over to the electromagnetic case; the decentralized vs. centralized analysis for the electromagnetic case is more complicated than for the acoustic case and does not seem to lead to easily generalized results.

5.2.2 An Example

As an example of the impact of using results from the wrong signal model, consider a signal that is a linear chirp signal having frequency sweep rate of α rad/sec^2: $s[n] = e^{j\varphi} e^{j(\alpha/2)(nT)^2}$. The correct FIM for a chirp signal would be computed using the results in Section 5.2.4 and can be shown to be [18]

$$\mathbf{J}_{right} = \begin{bmatrix} \alpha^2 & \alpha \\ \alpha & 1 \end{bmatrix}, \tag{60}$$

where the non-zero off-diagonal elements show that for this deterministic signal there is correlation between the TDOA and FDOA estimates. However, if one were to incorrectly use the uncorrelated TDOA/FDOA result that arises from the acoustic signal model (but still properly compute on-diagonal elements of the FIM) you'd get

$$\mathbf{J}_{wrong} = \begin{bmatrix} \alpha^2 & 0 \\ 0 & 1 \end{bmatrix}, \tag{61}$$

If we consider the case of two sensor pairs (no sharing of sensors between the pairs) with the same SNR at all sensors then the CRLB of the geolocation estimate is given by

$$\mathbf{CRLB}_{geo} = \left(\mathbf{H}_1^{\mathrm{T}} \mathbf{J} \mathbf{H}_1 + \mathbf{H}_2^{\mathrm{T}} \mathbf{J} \mathbf{H}_2 \right)^{-1}, \tag{62}$$

where H_i is the Jacobian matrix of the TDOA/FDOA measurements for the i^{th} sensor pair[13]. Taking the ratio of (62) evaluated using (60) to (62) evaluated using (61) gives a metric of the impact of using the incorrect uncorrelated TDOA/FDOA result.

The sensor/emitter geometry considered here is as follows: Emitter at $(x_e,y_e)=(0,0)$, Sensor Pair #1 at x,y positions of (-10,-50) and (10,-50) in km and both x,y velocities of (0,300) in m/s, Sensor Pair #2 at x,y positions of (50,-10) and (50,10) in km and both x,y velocities of (300 cos(θ), 300 sin(θ)) in m/s, where θ is the heading of each sensor in Sensor Pair #2. The surface plot in Figure 15 shows how the ratio of the two evaluations of (62) varies as a function of sweep rate α and Sensor Pair #2 heading θ; the range of heading angle is 0 to 360 degrees and the range for sweep rate is 10^4 to 10^8 rad/sec^2 (or about 1.6 kHz/sec to 16 MHz/sec), which are reasonable values for radar pulses. Note that a value near 1 for the plotted ratio shows that there is little impact in using the incorrect uncorrelated TDOA/FDOA result. Note that there are some conditions where there is little impact but there are many where the incorrect CRLB differs significantly, showing the importance of using the correct model's results. As α gets larger the ratio converges to 1; this is due to the fact that for very large α the α^2 term dominates the α off-diagonal terms in (60). Similarly, at lower values of α the off-diagonal terms in (60) have a negligible impact and the ratio is also effectively 1.

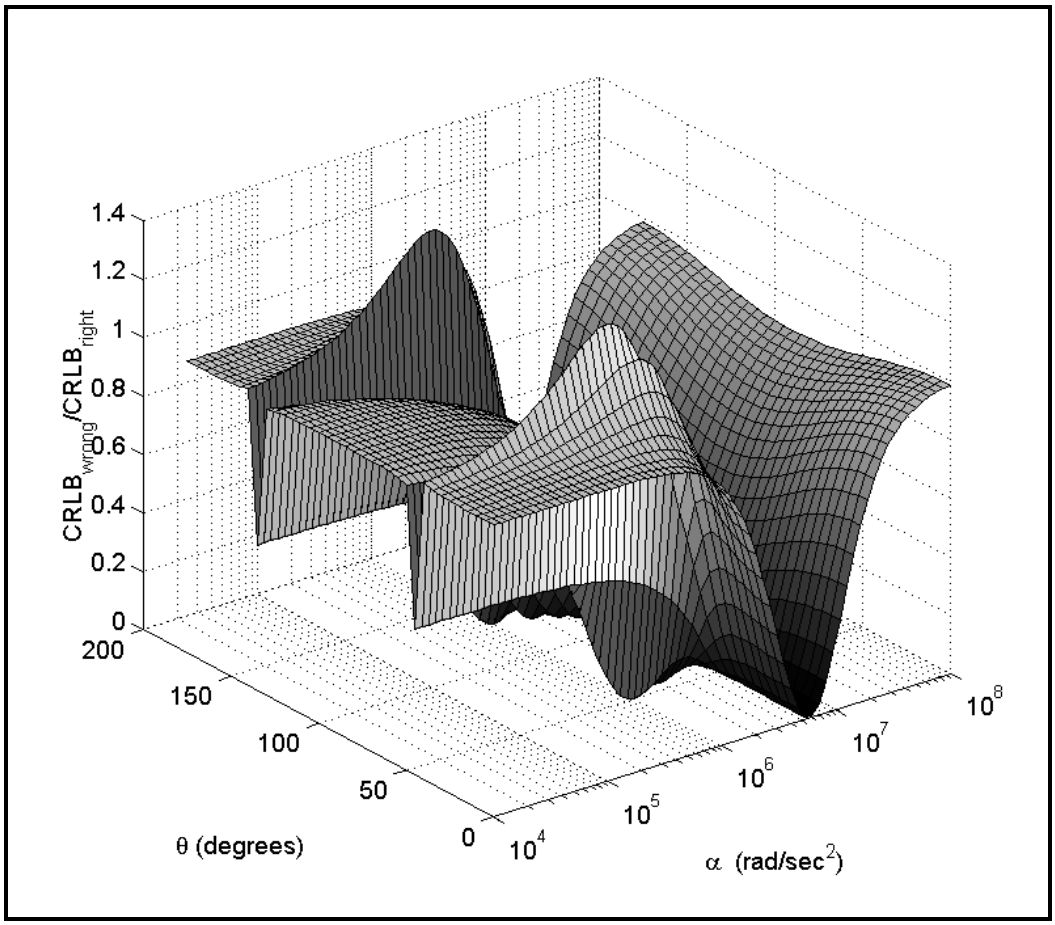

Figure 15: Ratio of the wrong $CRLB_{geo}$ to the right $CRLB_{geo}$ as a function of sweep rate α and heading θ of sensor pair #2.

5.2.3 Conclusions

The signal models for these two cases (passive acoustic and passive electromagnetic) may seem to be the same at a casual look (i.e., the equations in (45) are used in each case) but the underlying assumption about the signal (i.e., WSS Gaussian signal for the passive acoustic case and a deterministic signal for the passive electromagnetic case) leads to important differences in the results for the FIM, CRB, and MLE. The main differences are that: (i) the general structures of the FIM and CRB are significantly different; (ii) a key specific difference in the FIM/CRB structure is that unlike in the acoustic case, for the electromagnetic case the FDOA and TDOA estimates of a signal pair are likely to be correlated; (iii) for the electromagnetic case the MLE is an unfiltered cross-correlator whenever the noise is white (the acoustic case requires the signal to be white in order to remove the filters). Ignoring these differences can lead to incorrect location accuracy assessments as well as improper choices when developing processing schemes.

5.2.4 Derivation of FIM for Deterministic Signal Case

To evaluate the FIM in (51) for the deterministic-signal TDOA/FDOA case we need partial derivatives of the signal vector $\mathbf{s_\theta} = \begin{bmatrix} \mathbf{s}_1^T & \mathbf{s}_2^T \end{bmatrix}^T$. Using the signal model in (45) we get

$$\frac{\partial \mathbf{s_\theta}}{\partial \Delta_\tau} = \begin{bmatrix} \dfrac{\partial \mathbf{s}_1}{\partial \Delta_\tau} \\ \dfrac{\partial \mathbf{s}_2}{\partial \Delta_\tau} \end{bmatrix} = \begin{bmatrix} \left(\dfrac{\partial \mathbf{s}_1}{\partial \tau_1}\right) / \left(\dfrac{\partial \Delta_\tau}{\partial \tau_1}\right) \\ \left(\dfrac{\partial \mathbf{s}_2}{\partial \tau_2}\right) / \left(\dfrac{\partial \Delta_\tau}{\partial \tau_2}\right) \end{bmatrix} = \begin{bmatrix} \dfrac{\partial \mathbf{s}_1}{\partial \tau_1} \\ -\dfrac{\partial \mathbf{s}_2}{\partial \tau_2} \end{bmatrix} = \begin{bmatrix} -\mathbf{s}_1' \\ \mathbf{s}_2' \end{bmatrix} \tag{63}$$

where $\mathbf{s}_i'$ is the vector of samples of the time-derivative of the received signal; we have used the chain rule here and the fact that $\partial s(nT - \tau_i) / \partial \tau_i = -ds(t)/dt\big|_{t=nT-\tau_i}$. Similarly we have

$$\frac{\partial \mathbf{s_\theta}}{\partial \Delta_v} = \begin{bmatrix} \dfrac{\partial \mathbf{s}_1}{\partial \Delta_v} \\ \dfrac{\partial \mathbf{s}_2}{\partial \Delta_v} \end{bmatrix} = \begin{bmatrix} \dfrac{\partial \mathbf{s}_1}{\partial v_1} \\ -\dfrac{\partial \mathbf{s}_2}{\partial v_2} \end{bmatrix} = \begin{bmatrix} \tilde{\mathbf{s}}_1 \\ -\tilde{\mathbf{s}}_2 \end{bmatrix} \tag{64}$$

where $\tilde{\mathbf{s}}_i$ is the vector with elements that are the elements of $\mathbf{s}_i$ multiplied by the corresponding jnT with n running sequentially over its range. Using these results in (51) gives

$$\left[\mathbf{J}_{em}\right]_{11} = 2\,\mathrm{Re}\left\{ \begin{bmatrix} -\mathbf{s}_1' \\ \mathbf{s}_2' \end{bmatrix}^H \mathbf{C}^{-1} \begin{bmatrix} -\mathbf{s}_1' \\ \mathbf{s}_2' \end{bmatrix} \right\} = 2\,\mathrm{Re}\left\{ \mathbf{s}_1'^H \mathbf{C}_1^{-1} \mathbf{s}_1' + \mathbf{s}_2'^H \mathbf{C}_2^{-1} \mathbf{s}_2' \right\}, \tag{65}$$

$$\left[\mathbf{J}_{em}\right]_{22} = 2\,\mathrm{Re}\left\{ \begin{bmatrix} \tilde{\mathbf{s}}_1 \\ -\tilde{\mathbf{s}}_2 \end{bmatrix}^H \mathbf{C}^{-1} \begin{bmatrix} \tilde{\mathbf{s}}_1 \\ -\tilde{\mathbf{s}}_2 \end{bmatrix} \right\} = 2\,\mathrm{Re}\left\{ \tilde{\mathbf{s}}_1^H \mathbf{C}_1^{-1} \tilde{\mathbf{s}}_1 + \tilde{\mathbf{s}}_2^H \mathbf{C}_2^{-1} \tilde{\mathbf{s}}_2 \right\}, \tag{66}$$

$$\left[\mathbf{J}_{em}\right]_{12} = \left[\mathbf{J}_{em}\right]_{21} = 2\,\mathrm{Re}\left\{ \begin{bmatrix} -\mathbf{s}_1' \\ \mathbf{s}_2' \end{bmatrix}^H \mathbf{C}^{-1} \begin{bmatrix} \tilde{\mathbf{s}}_1 \\ -\tilde{\mathbf{s}}_2 \end{bmatrix} \right\} = 2\,\mathrm{Re}\left\{ -\mathbf{s}_1'^H \mathbf{C}_1^{-1} \tilde{\mathbf{s}}_1 - \mathbf{s}_2'^H \mathbf{C}_2^{-1} \tilde{\mathbf{s}}_2 \right\}, \tag{67}$$

where $\mathbf{C}_i$ is the covariance of the i^{th} noise process. For white noise with noise variances of σ_i^2 we get

$$\left[\mathbf{J}_{em}\right]_{11} = \frac{2}{\sigma_1^2} \sum_n \left| s'(nT - \tau_1) \right|^2 + \frac{2}{\sigma_2^2} \sum_n \left| s'(nT - \tau_2) \right|^2, \tag{68}$$

$$\left[\mathbf{J}_{em}\right]_{22} = \frac{2T}{\sigma_1^2} \sum_n n^2 \left| s(nT - \tau_1) \right|^2 + \frac{2}{\sigma_2^2} \sum_n n^2 \left| s(nT - \tau_2) \right|^2, \tag{69}$$

$$[\mathbf{J}_{em}]_{12} = [\mathbf{J}_{em}]_{21} = 2\,\mathrm{Re}\left\{ \frac{1}{\sigma_1^2} \sum_n -jnTs^*(nT-\tau_1)s'(nT-\tau_1) + \frac{1}{\sigma_2^2} \sum_n -jnTs^*(nT-\tau_2)s'(nT-\tau_2) \right\}. \quad (70)$$

Note that in the $[\mathbf{J}_{em}]_{22}$ element for the FDOA the signal samples are quadratically weighted by time. A dual result for the $[\mathbf{J}_{em}]_{11}$ element for the TDOA can be developed where the signal's DFT values are quadratically weighted by frequency; this can be obtained from (68) by using Parseval's theorem and properties of Fourier transforms or can be obtained by using a frequency domain formulation of the signal data as is done in 6. These quadratically weighted relationships are similar to such weightings shown in the CRB results for the continuous-time case stated in [9] without proof.

6 References

[1] M. Chen, M. L. Fowler, A. Noga, "Data compression for simultaneous/sequential inference tasks in sensor networks," IEEE ICASSP 2006, Toulouse, France, May 2006.

[2] N. Christofides, A. Mingozzi, P. Toth and C. Sandi, Combinatiorial Optimization, Wiley-Interscience, 1979

[3] W. R. Hann and S. A. Tretter, "Optimum processing for delay-vector estimation in passive signal arrays," *IEEE Trans. Information Theory*, vol. IT-19, pp. 608 - 614, Sept. 1973.

[4] W. R. Hann, "Optimum signal processing for passive sonar range and bearing estimation," *J. Acoust. Soc. Am.*, Vol. 58 pp. 201 – 207, July 1975.

[5] C. H. Knapp and G. C. Carter, "The generalized correlation method for estimation of time delay," *IEEE Trans. Acoust., Speech, and Signal Processing*, vol. ASSP-24, pp. 320 - 327, Aug. 1976.

[6] P. M. Schultheis and E. Weinstein, "Estimation of differential Doppler shifts," *J. Acoust. Soc. Am.*, Vol. 66 pp. 1412 – 1419, Nov. 1979.

[7] G. C. Carter, "Time delay estimation for passive sonar signal processing," *IEEE Trans. Acoust., Speech, and Signal Processing*, vol. ASSP-29, pp. 463 - 470, June 1981.

[8] A. H. Quazi, "An overview on the time delay estimate in active and passive systems for target localization," *IEEE Trans. Acoust., Speech, and Signal Processing*, vol. ASSP-29, pp. 527 - 533, June 1981.

[9] S. Stein, "Algorithms for ambiguity function processing," *IEEE Trans. Acoust., Speech, and Signal Processing*, vol. ASSP-29, pp. 588 - 599, June 1981.

[10] E. Weinstein, "Decentralization of the Gaussian maximum likelihood estimator and its application to passive array processing," *IEEE Trans. Acoust., Speech, and Signal Processing*, vol. ASSP-29, pp. 945 - 951, Oct. 1981.

[11] P. C. Chestnut, "Emitter location accuracy using TDOA and differential doppler ," *IEEE Trans. Aero. and Electronic Systems*, vol. AES-18, pp. 214-218, March 1982.

[12] M. Wax, "The joint estimation of differential delay, Doppler, and phase," *IEEE Trans. Information Theory*, vol. IT-28, pp. 817 - 820, Sept. 1982.

[13] D. J. Torrieri, "Statistical theory of passive location system," *IEEE Trans. on Aerosp. Elect. Syst.*, vol. AES-20, no. 2, March 1984, pp. 183 – 198.

[14] B. Friedlander, "On the Cramer-Rao bound for time delay and Doppler estimation," *IEEE Trans. Information Theory*, vol. IT-30, pp. 575 - 580, May 1984.

[15] T. Berger and R. Blahut, "Coherent estimation of differential delay and differential Doppler," *Proc. ofConf. on Information Sciences and Systems*, Princeton University, pp. 537 – 541,1984.

[16] S. Stein, "Differential delay/Doppler ML estimation with unknown signals," *IEEE Trans. Signal Processing*, vol. 41, pp. 2717-2719, August 1993.

[17] S. Kay, *Fundamentals of Statistical Signal Processing: Estimation Theory*, Prentice Hall, 1993.

[18] M. L. Fowler and M. Chen, "Evaluating Fisher Information From Data for Task-Driven Data Compression," *Proceedings of Conference on Information Sciences and Systems*, Princeton University, March 22-24, 2006, pp. 976 – 972.

[19] Xi Hu, Mo Chen, and M. L. Fowler, "Exploiting Data Compression Methods for Network-Level Management of Multi-Sensor Systems," *Proceedings of SPIE - The International Society for Optical Engineering*, v 6315, *Mathematics of Data/Image Pattern Recognition, Compression, and Encryption with Applications IX*, 2006.

[20] M. L. Fowler and M. Chen, "Fisher-information-based data compression for estimation using two sensors," *IEEE Transactions on Aerospace and Electronic Systems*, vol. 41, no. 3, July 2005, pp. 1131 - 1137.